

# **North Pacific Climate Response to Freshwater Forcing in the Subarctic North Atlantic: Oceanic and Atmospheric Pathways**

Yuko M. Okumura\*, Clara Deser, and Aixue Hu

*Climate and Global Dynamics Division, National Center for Atmospheric Research  
Boulder, Colorado, USA*

Axel Timmermann and Shang-Ping Xie

*International Pacific Research Center, University of Hawaii at Manoa  
Honolulu, Hawaii, USA*

*Journal of Climate*

February 28, 2008, submitted

August 1, 2008, revised

\* Corresponding author address:

Dr. Yuko M. Okumura

Climate and Global Dynamics Division  
National Center for Atmospheric Research  
P.O. Box 3000, Boulder, Colorado 80307, USA

Tel: (303) 497-1770

Fax: (303) 497-1333

E-mail: yukoo@ucar.edu

## Abstract

Sudden changes of the Atlantic meridional overturning circulation (AMOC) are believed to have caused large, abrupt climate changes over many parts of the globe during the last glacial and de-glacial period. This study investigates the mechanisms by which a large freshwater input to the subarctic North Atlantic and an attendant rapid weakening of the AMOC influence North Pacific climate by analyzing four different ocean-atmosphere coupled general circulation models (GCMs) under present-day or pre-industrial boundary conditions. When the coupled GCMs are forced with a 1 Sv freshwater flux anomaly in the subarctic North Atlantic, the AMOC nearly shuts down and the North Atlantic cools significantly. The South Atlantic warms slightly, shifting the Atlantic intertropical convergence zone southward. In addition to this Atlantic ocean-atmosphere response, all the models exhibit cooling of the North Pacific, especially along the oceanic frontal zone, and deepening of the wintertime Aleutian Low, consistent with paleoclimate reconstructions.

Detailed analysis of one coupled GCM identifies both oceanic and atmospheric pathways from the Atlantic to the North Pacific. The oceanic teleconnection contributes a large part of the North Pacific cooling: the freshwater input to the North Atlantic raises sea level in the Arctic Ocean and reverses the Bering Strait throughflow, transporting colder, fresher water from the Arctic Ocean into the North Pacific. When the Bering Strait is closed, the cooling is greatly reduced while the Aleutian Low response is enhanced. Tropical SST anomalies in both the Atlantic and Pacific are found to be important for the equivalent barotropic response of the Aleutian Low during boreal winter. The atmospheric bridge from the tropical North Atlantic is particularly important, and quite sensitive to the mean state, which is poorly simulated in many coupled GCMs. The enhanced Aleutian Low, in turn, cools the North Pacific by increasing

surface heat fluxes and southward Ekman transport. The closure of the Bering Strait during the last glacial period suggests that the atmospheric bridge from the tropics and air-sea interaction in the North Pacific played a crucial role in the AMOC-North Pacific teleconnection.

## 1. Introduction

In contrast to the relatively stable climate of the last 10 kyr, the recent glacial and deglacial period (~10-110 kyr ago) was marked by large, rapid climate variations on millennial time scales, as revealed by isotope analyses of Greenland ice cores (Dansgaard et al. 1993; see Weart 2003 for a historical account) and other proxies. Surface air temperature in Greenland repeatedly underwent periods of abrupt warming followed by more gradual cooling, with amplitudes of 5°-10°C. Some temperature jumps occurred in less than a century or even a decade. Some of the cold periods in Greenland are also marked by layers of ice-rafted debris in the North Atlantic Ocean sediment cores that indicate increased discharge of continental ice into the ocean (Heinrich 1988; Bond and Lotti 1995).

Growing evidence from subsequent studies shows that these rapid climate changes were not confined to the North Atlantic but spread over many parts of the world. During the Greenland cold phases, the Atlantic intertropical convergence zone (ITCZ) was displaced southward (Peterson et al. 2000; Wang et al. 2004; Schmidt et al. 2006), Indian and Asian summer monsoons were weakened (Wang et al. 2001; Altabet et al. 2002; Ivanochko et al. 2005), and the eastern equatorial Pacific was colder (Koutavas et al. 2002; Kienast et al. 2006) with the Pacific ITCZ displaced southward (Leduc et al. 2007) and the Walker circulation weakened (Stott et al. 2002). Outside the tropics, large SST variations closely related to the Greenland records are reported in different parts of the North Pacific (Thunell and Mortyn 1995; Hendy and Kennett 1999; Kienast and McKay 2001) and the Okhotsk Sea (Harada et al. 2006). Enhanced ventilation during the cold periods is also suggested in the analyses of ocean sediments from the Santa Barbara basin (Behl and Kennett 1996) and the Northeast Pacific (Lund and Mix 1998). For atmospheric circulation, recent analysis of lake sediments shows decreased (increased)

moisture availability in the western (central) part of southern Alaska during the Younger Dryas, implying that the Aleutian Low was stronger compared to present-day (D. S. Kaufman 2008, personal communication; see Hu et al. 2006 for the analysis of lake sediments from southwestern Alaska).

The Atlantic meridional overturning circulation (AMOC, aka. thermohaline circulation) is considered to have played a central role in the millennial climate variations during the last glacial period. In present-day climate, ocean surface current carries warm, saline tropical water toward the extratropical North Atlantic, where the water cools, sinks, and returns southward at depth, transporting a large amount of heat into high latitudes. Models with various complexity suggest that the AMOC is sensitive to a change in extratropical surface buoyancy, particularly salinity fluxes (e.g., Stommel 1961; Bryan 1986; Manabe and Stouffer 1988; Mikolajewicz and Maier-Reimer 1994; Rahmstorf 1995; Schiller et al. 1997; Yin and Stouffer 2007). A large freshwater flux anomaly due to melting icebergs or glacial discharge increases the surface buoyancy and can inhibit deepwater formation in the North Atlantic. As a result, the AMOC shuts down temporally or reaches another state of equilibrium. Rooth (1982) and Broecker (1985) are among the first studies to propose the connection between rapid climate changes and the AMOC. Their idea has been supported by a number of paleoclimate studies indicating that reduced production of North Atlantic deepwater was accompanied by stadial conditions in the North Atlantic region (Boyle and Keigwin 1987; Oppo and Lehman 1995; McManus et al. 2004).

While it is straightforward to understand the impact of an AMOC shutdown on surface temperatures in the extratropical North Atlantic via oceanic heat transport (Krebs and Timmermann 2007), it is not fully understood how climate in distant regions can be affected. Ocean models successfully simulate the North Atlantic cooling when the AMOC is forced to

collapse, but surface temperature anomalies are mostly confined to the North Atlantic (e.g., Mikolajewicz and Maier-Reimer 1994), suggesting an important role of the atmospheric circulation in conveying an AMOC change beyond the Atlantic basin. Indeed, the pioneering coupled GCM study by Manabe and Stouffer (1988) showed that the climatic impact of an AMOC shutdown can be global. In response to a shutdown of the AMOC, the extratropical North Atlantic cools up to  $-7^{\circ}\text{C}$  and the South Atlantic warms slightly. Associated with this north-south dipole of temperature anomalies, the Atlantic ITCZ shifts southward, consistent with paleoclimate records. The cooling is not confined to the North Atlantic but spread over the entire Northern Hemisphere. These features are also robust in subsequent coupled GCM studies, although the degree of AMOC stability is strongly model-dependent (Schiller et al. 1997; Dong and Sutton 2002; Vellinga and Wood 2002; Zhang and Delworth 2005; Stouffer et al. 2006; Timmermann et al. 2007; Wu et al. 2008).

For a quantitative comparison of the climate response to freshwater water perturbations and resultant AMOC changes among different coupled GCMs, coordinated “water-hosing” experiments were conducted as part of Coupled Model Intercomparison Project/Paleo-Modeling Intercomparison Project (CMIP/PMIP; Stouffer et al. 2006). In response to 1 Sv freshwater forcing in the subarctic North Atlantic, the AMOC slows down rapidly in all of the models and associated climatic anomalies exhibit a large degree of similarity, especially in the Atlantic basin: a north-south dipole pattern of surface temperature anomalies and southward displacement of the ITCZ. While a change in oceanic heat transport is fundamental for this interhemispheric surface temperature dipole (Yang 1999; Knutti et al. 2004; Wu et al. 2008), atmospheric teleconnections from the extratropics and tropical air-sea interaction also play an important role (Chiang and Bitz 2005; Krebs and Timmermann 2007; Chiang et al. 2008).

The AMOC-induced climate anomalies in the Atlantic further influence the other tropical basins through atmospheric teleconnections. In response to a substantial weakening of the AMOC, the eastern Pacific ITCZ is displaced southward (Dong and Sutton 2002; Vellinga and Wood 2002; Zhang and Delworth 2005; Timmermann et al. 2007; Wu et al. 2008). The tropical North Atlantic cooling induces anomalous high pressure that extends westward into the eastern tropical North Pacific, thereby intensifying northeasterly trades across the Central American Isthmus. These cross-Isthmus winds advect anomalously cold and dry air from the Atlantic and decrease SST in the eastern tropical North Pacific by enhancing surface turbulent heat fluxes, mixing, and upwelling with a distinct seasonality (Zhang and Delworth 2005; Xie et al. 2008). As a result of subsequent air-sea interactions in the tropical Pacific, some models develop an El Niño or La Niña-like SST anomaly pattern with an equatorial maximum (Dong and Sutton 2002; Wu et al. 2008) whereas other models favor a meridional dipole pattern similar to that in the tropical Atlantic (Vellinga and Wood 2002; Zhang and Delworth 2005). The associated reduction in meridional SST gradient suppresses the annual cycle in the eastern equatorial Pacific, which may lead to an enhanced El Niño-Southern Oscillation (ENSO) via nonlinear frequency entrainment (Timmermann et al. 2007). Zhang and Delworth (2005) also suggest that an adjustment of Walker circulation leads to weakened Indian and Asian monsoons. These tropical responses are in general agreement with the paleoclimate studies mentioned earlier.

Beyond the Atlantic basin, coupled GCMs also exhibit a robust response over the North Pacific (Timmermann et al. 2007). When the AMOC nearly shuts down, the North Pacific cools throughout the basin with maximum amplitude of 3°-5°C along the oceanic frontal zone, and westerly winds intensify associated with deepening of the wintertime Aleutian Low. This North Pacific response appears in many earlier coupled GCM studies (e.g., Manabe and Stouffer 1988;

Mikolajewicz et al. 1997; Schiller et al. 1997; Dong and Sutton 2002; Vellinga and Wood 2002; Zhang and Delworth 2005) and agrees with paleoclimate records, suggesting a strong connection between the AMOC and North Pacific climate. However, few studies address the mechanisms of this inter-basin teleconnection. Manabe and Stouffer (1988) explain the North Pacific cooling by thermal advection of the North Atlantic temperature anomalies by prevailing westerly winds. The advected cold air enhances upward surface heat fluxes in the North Pacific and the resultant SST cooling, in turn, intensifies the westerly winds by thermal wind balance. If thermal advection is the dominant mechanism for the North Pacific cooling, it is expected that the magnitude of surface temperature anomalies decreases toward the east across the Eurasian continent and North Pacific. In most of the models, however, the North Pacific cooling is larger than the surface air temperature anomalies in the Far East by a few degrees.

The deepened Aleutian Low appears to be the key to understand this North Pacific response in addition to thermal advection: anomalous northerly winds advect colder Arctic air in the western basin, while enhanced westerlies increase upward surface heat fluxes and southward Ekman transport in the central basin; furthermore, the positive wind stress curl may act to shift the oceanic front to the south, all intensifying the SST cooling. In the most comprehensive study on this subject to date, Mikolajewicz et al. (1997) show that the atmospheric circulation anomaly in their water-hosing experiment projects strongly on the leading internal mode over the North Pacific sector, which represents changes in the strength and position of the Aleutian Low. They suggest that the Aleutian Low response is a combination of remote influence from the Atlantic and local air-sea interactions in the North Pacific. Using a “partial-coupling” technique in a coupled GCM, Wu et al. (2008) argue that the extratropical North Atlantic cooling is the major driver for the North Pacific response. In their model, the strong North Atlantic cooling

accelerates westerly winds over the North Pacific by triggering a positive phase of the annular mode (Thompson and Wallace 2000). However, the low pressure and westerly wind anomalies associated with the annular mode patterns are limited to north of the subarctic North Pacific and thus this mechanism does not explain the stationary wave feature of the Aleutian Low that extends into the mid-latitude North Pacific. The large tropical heating anomalies associated with changes in the Atlantic and Pacific ITCZs are likely to influence the extratropical atmospheric circulation by exciting barotropic Rossby waves (Hoskins and Karoly 1981), but their role has not been investigated in association with the AMOC change explicitly.

Given the rapid rate of North Pacific SST changes associated with the North Atlantic climate anomalies (Thunell and Mortyn 1995; Hendy and Kennett 1999; Kienast and McKay 2001), atmospheric teleconnections are likely to have played a crucial role in the AMOC-North Pacific linkage during the last glacial period. Oceanic teleconnections, however, cannot be dismissed. Hu and Meehl (2005) and Hu et al. (2007; 2008) show that a part of the freshwater flux anomaly applied to the North Atlantic is transported into the North Pacific through the Bering Strait by reversing the hydraulically-controlled throughflow. This inflow of cold and fresh Arctic water may have a significant impact on the heat and salinity balance in the North Pacific. With a depth of 30-50 m and a width of 85-150 km, the Bering Strait was closed during the last glacial period due to snow/ice accumulation over the continents and resultant decrease in sea level (Chappell 2002; Siddall et al. 2003). Therefore, such an oceanic teleconnection is not relevant to the millennial-scale climate variations during the last glacial period but its impact needs to be evaluated in models since most of previous coupled GCM studies use the present-day boundary condition (i.e., an open Bering Strait). The open Bering Strait experiment may also be applicable to the short-lived cold event that occurred approximately 8.2 kyr ago during the

Holocene although the associated freshwater discharge of 5-10 Sv lasted less than a year (Clarke et al. 2003). Slow adjustment of the global thermohaline circulation and transmission of oceanic waves influence the North Pacific as well (e.g., Manabe and Stouffer 1997; Mikolajewicz et al. 1997; Timmermann et al. 2005a). It is suggested that the intermediate/deep water formation tends to resume in the North Pacific when the Atlantic MOC is suppressed (Saenko et al. 2004; Timmermann et al. 2005b; Krebs and Timmermann 2007; Mikolajewicz et al. 2007). This inter-basin seesaw may explain the out-of-phase temperature variations between the subarctic North Pacific and Atlantic implied by a few paleoclimate studies (Kiefer et al. 2001; Sarnthein et al. 2006). In an uncoupled ocean model experiment, however, a change in the North Pacific ventilation is reduced to one third of that in a coupled experiment (Mikolajewicz et al. 1997), suggesting again a dominant role of the atmospheric teleconnections which can spread the Atlantic climate change much faster than the oceanic processes can accomplish alone.

In the present study, we revisit the unresolved issues of the linkage between the AMOC and North Pacific climate. How consistent is the North Pacific climate response to a rapid weakening of the AMOC among coupled GCMs in terms of its magnitude, seasonality, and temporal evolution? What are the oceanic and atmospheric dynamical processes involved in the teleconnection besides atmospheric thermal advection? How does a change in the Bering Strait throughflow affect the North Pacific? What are the mechanisms for the Aleutian Low response, and how does the enhanced Aleutian Low impact the North Pacific? To approach these problems, we first analyze the CMIP/PMIP water-hosing experiments with four different coupled GCMs (Section 3). By identifying common features of the North Pacific response and its relation to changes in other regions, the roles of oceanic and atmospheric teleconnections can be inferred. The hypothesized mechanisms are tested in additional experiments with one particular coupled

GCM and its atmospheric component (Section 4). The oceanic teleconnection is examined by comparing two sets of water-hosing experiments, one with an open Bering Strait and one with a closed Bering Strait (Subsection 4.1). The origin of the atmospheric teleconnection is explored in a series of atmospheric GCM experiments forced by SST anomalies simulated in the coupled GCM water-hosing experiment (Subsection 4.2). The description of models and experiments is provided in Section 2. The last section summarizes the main results of this study and discusses their implications and remaining issues.

## **2. Models and experiments**

### *a. CMIP/PMIP water-hosing experiments*

A subset of the CMIP/PMIP water-hosing experiments is analyzed to identify common, robust features of the AMOC-North Pacific teleconnection among different models. In these coordinated experiments, coupled GCMs are forced with a time-invariant freshwater flux anomaly in the subarctic North Atlantic (50°-70°N) for 100 years. The freshwater flux is evenly distributed over the broad forcing area to account for model-to-model variations in the location of deep convection. In reality, the freshwater discharge was likely to be more localized near the continental boundaries, which may affect the climate response (Saenko et al. 2007). We examine the case of 1 Sv hosing for which the AMOC nearly shuts down in all the models (Stouffer et al. 2006). This rate will increase the global-mean sea level by 9 m over a 100-year period. Comparable sea level changes are estimated for the millennium climate variations during the last glacial period although they took place over a longer period (Chappell 2002; Siddall et al. 2003; Clark et al. 2004). The integration is continued without freshwater forcing for an additional 100 years or longer, allowing the climate system to recover. In this paper, we focus on the coupled GCMs' responses during the first and last several decades of the 100-year hosing period.

Although it takes longer than 100 years for the global thermohaline circulation to equilibrate with the freshwater forcing, the climate response develops very rapidly during the first few decades due to atmospheric teleconnections as will be shown in the following sections. The climatic impact of the freshwater forcing and resultant AMOC change is assessed by comparing the hosing run to climatologies of a 200-year control simulation for each model. All the models use present-day or pre-industrial boundary conditions and therefore the Bering Strait is open, connecting the Atlantic and Pacific through the Arctic Ocean.

Four different coupled GCMs are presented: the National Center for Atmospheric Research Community Climate System Model version 2.0 (CCSM2; Kiehl and Gent 2004), Max Planck Institute for Meteorology atmosphere-ocean model (ECHAM5-OM1; Jungclaus et al. 2006), Geophysical Fluid Dynamics Laboratory Climate Model version 2.1 (GFDL\_CM2.1; Delworth et al. 2006), and Hadley Centre Coupled Ocean–Atmosphere General Circulation Model version 3 (HadCM3; Gordon et al. 2000). These state-of-the-art climate models are comprised of ocean/atmosphere GCMs and land surface/sea ice models, and maintain stable climates without flux adjustment in the control simulations. The ECHAM5-OM1, GFDL\_CM2.1, HadCM3, and the subsequent version of CCSM2 (CCSM3) have been used in a recent assessment report by the Intergovernmental Panel on Climate Change (IPCC) and their simulations of mean climate are highly ranked among other models (Reichler and Kim 2008), thus well representing the current generation of coupled GCMs. The horizontal resolutions of ocean/atmosphere GCMs are  $1.1^\circ \times (0.27^\circ\text{-}0.6^\circ)/T42$  ( $\sim 2.8^\circ$ ) in CCSM2,  $3^\circ \times 3^\circ/T31$  ( $\sim 3.75^\circ$ ) in ECHAM5-OM1,  $1^\circ \times (1/3^\circ\text{-}1^\circ)/2.5^\circ \times 2^\circ$  in GFDL\_CM2.1, and  $1.25^\circ \times 1.25^\circ/3.75^\circ \times 2.5^\circ$  in HadCM3. Note that CCSM2 and HadCM3 use virtual salt flux instead of real water flux in the water-hosing experiments without a global salinity compensation. The next subsection describes CCSM2 in

more detail. Further information on the other three models and the experimental setting are provided in Stouffer et al. (2006), Timmermann et al. (2007), and the above references for individual models.

*b. CCSM2 and CAM2*

The oceanic and atmospheric teleconnection processes are examined through additional experiments with CCSM2 and its atmospheric component, Community Atmosphere Model version 2 (CAM2; a model description is available online at <http://www.cesm.ucar.edu/models/atm-cam/>). CAM2 is a global GCM with an Eulerian spectral dynamical core and a comprehensive physical package. Both stand-alone CAM2 and CCSM2 simulations use a version with triangular truncation at T42 ( $\sim 2.8^\circ$ ) and 26 hybrid vertical levels. The ocean component is based upon the Parallel Ocean Program (POP) developed at Los Alamos National Laboratory. POP has 40 vertical levels and a horizontal resolution of  $\sim 1.1^\circ \times (0.27^\circ\text{-}0.6^\circ)$  with the northern pole displaced into Greenland. CCSM2 also includes the Community Land Model version 2 (CLM2) and the Community Sea Ice Model version 4 (CSIM4), which have horizontal grids identical to those of CAM2 and POP, respectively. These four components are linked by means of a flux coupler.

In addition to the CMIP/PMIP experiment described in the previous subsection, another water-hosing experiment is conducted with CCSM2. This experiment is identical to the previous one except that the Bering Strait is closed, preventing water mass exchange between the North Pacific and the Arctic Ocean. The control simulation is also repeated with the Bering Strait closed. The AMOC in these two experiments is analyzed in detail by Hu and Meehl (2005) and Hu et al. (2007; 2008). By comparing the North Pacific response in the open and closed Bering Strait cases, the roles of oceanic and atmospheric teleconnections can be assessed.

To examine the atmospheric teleconnection processes in more detail, a series of CAM2 simulations is conducted by prescribing SST and sea ice fraction fields simulated in the *closed* Bering Strait experiment. First, CAM2 is forced with monthly climatologies of SST and sea ice from the 200-year control run of CCSM2 in the closed Bering Strait configuration. Monthly SST and sea ice anomalies averaged over the last 30 years of the 100-year hosing period are then added in different regions: the extratropical North Atlantic (40°-75N), tropical Atlantic (25°S-30°N), entire Atlantic (25°S-75°N), or entire Atlantic (25°S-75°N) and tropical Pacific (15°S-15°N) combined. Outside these regions, a linear smoothing is applied to 10° latitude bands. Each of these CAM2 experiments is integrated for 30 years after a 4-month spin-up. Since year-to-year variability in these experiments is purely due to internal atmospheric dynamics, each year's simulation is treated as an independent sample in tests of statistical significance.

### **3. Coupled GCMs' response to 1 Sv freshwater forcing in the subarctic North Atlantic**

The AMOC intensity, defined here as the maximum meridional overturning stream function value in the North Atlantic, ranges from 15 to 23 Sv in the control runs of the four coupled GCMs (Stouffer et al. 2006; Timmermann et al. 2007). The AMOC is vigorous and presents pronounced multidecadal variations in GFDL\_CM2.1 and HadCM3 while both the mean intensity and multidecadal variations are relatively weak in CCSM2 and ECHAM5-OM1. In response to 1 Sv freshwater forcing in the North Atlantic, all the models exhibit a rapid weakening of the AMOC during the first few decades. The AMOC reaches a near-equilibrium, collapsed state within 50 years with the intensity reduced to 2.5-6 Sv.

Figure 1 shows annual-mean SST, surface wind stress, and precipitation anomaly fields averaged over the last 30 years of the hosing period for the four coupled GCMs. The Atlantic response is very robust and consistent among the models. The extratropical North Atlantic SST

exhibits strong cooling of 8°-12°C which extends from the eastern basin into the subtropical North Atlantic. The South Atlantic warms slightly with maximum amplitude of 1°-3°C off the Angola-Namibia coast. Associated with this interhemispheric dipole pattern of SST anomalies, anomalous northerly winds blow across the equator and the Atlantic ITCZ is displaced toward the warmer Southern Hemisphere. The Coriolis force acting on these northerlies induces an anomalous easterly (westerly) component north (south) of the equator, enhancing (reducing) the easterly trade winds and associated latent heat loss from the sea surface. This tropical Atlantic anomaly pattern bears a close resemblance to decadal-interdecadal variations in present-day climate in which thermodynamic ocean-atmosphere interaction among wind, evaporation, and SST plays an important role (Xie and Carton 2004).

The models also exhibit a robust response in the North Pacific (Fig. 1). Maximum SST cooling of 3°-5°C occurs along 40°-45°N, near the climatological oceanic frontal zone in these models. In CCSM2 strong cooling east of the Kamchatka Peninsula extends southeastward and along the oceanic front east of 160°E. The GFDL\_CM2.1 and ECHAM5-OM1 show a sharp meridional SST gradient extending from the east coast of northern Japan across the basin, indicative of a southward shift of the oceanic front. Indeed, the position of the zero wind stress curl line is displaced southward in these models (not shown). Westerly winds strengthen over the cooling region in association with a cyclonic circulation anomaly. The largest wind anomalies are collocated with the maximum SST cooling in ECHAM5-OM1, GFDL\_CM2.1, and HadCM3 but displaced slightly to the north in CCSM2. These ocean-atmosphere anomalies are reminiscent of the pattern associated with the North Pacific interdecadal variability (e.g., Trenberth and Hurrell 1994; Mantua et al. 1997; Deser et al. 2004a). However, while intensified southerly winds induce positive temperature anomalies over the Gulf of Alaska in the

interdecadal variations, both air temperature and SST anomalies are weakly negative in the water-hosing experiments. The overall cooling of the Northern Hemisphere is likely to mask the regional warming in the eastern North Pacific in the water-hosing experiments.

The tropical Pacific displays a generally consistent response despite some differences among the models (Fig. 1). All the models simulate strengthening of the northeasterly trades across the Central American Isthmus. These enhanced northeasterly winds cool the northeast tropical Pacific by advecting anomalously cold, dry air from the North Atlantic and triggering local air-sea interactions (Xie et al. 2008). The CCSM2, GFDL\_CM2.1, and HadCM3 develop a meridional dipole pattern of SST anomalies in the eastern basin with anomalous cross-equatorial northerly winds and southward displaced ITCZ, much like that in the tropical Atlantic. The ECHAM5\_OM1, on the other hand, shows La Niña-like SST anomalies that peak at the equator. Precipitation anomalies in this model are much smaller compared to the other three models, which may be due to the lower resolution of its atmospheric component (T31). In the western basin, all models show suppressed deep convection over the maritime continent, suggesting a weakening of the Walker circulation. Peculiar to HadCM3 is a large precipitation increase in the western-central tropical North Pacific associated with weak SST warming.

The consistency of the North Pacific response in these coupled GCMs motivates us to study its mechanisms. We begin by examining the temporal evolution of ocean-atmosphere anomalies. Figure 2 presents latitude-time sections of annual-mean SST, surface wind stress, and precipitation anomalies averaged zonally in the Atlantic and Pacific and smoothed with a 7-year running mean filter. The extratropical North Atlantic cools very rapidly after the hosing starts, reaching 70-90% amplitude of the equilibrium response by the end of the first decade. The North Pacific cooling is as rapid as the North Atlantic cooling, but delayed by one decade, with the

largest change occurring during the second decade. The rapidity and distinct spatial structure of this remote response imply that dynamical processes are involved beside atmospheric thermal advection that undergoes diffusion and damping while traveling across the Eurasian continent. The North Pacific cooling is not preceded by westerly wind anomalies and they tend to develop simultaneously except in ECHAM5\_OM1 for which westerly wind anomalies associated with multidecadal variations appear to lead the SST cooling. A close examination of SST and wind anomaly maps shows that the frontal cooling begins before the westerly wind and cyclonic circulation anomalies become organized in all the models (not shown), suggesting an important role for oceanic processes in initiating the rapid SST cooling. An ensemble simulation is necessary to fully assess the nature of the causality between North Pacific SST and surface wind changes due to the presence of atmospheric “noise” associated with ENSO and internal atmospheric variability in a single model realization.

The wind anomalies are likely to enhance the North Pacific cooling through changes in surface heat fluxes and oceanic currents. These wind anomalies may be remotely forced by changes in tropical atmospheric convection or extratropical surface cooling. Both the tropical Atlantic and Pacific ocean-atmosphere anomalies develop during the second decade, coincident with the North Pacific response (Fig. 2). The Atlantic anomalies remain nearly steady after year 20-30 except in HadCM3 for which SST, surface wind, and precipitation anomalies all gradually increase throughout the hosing period. The cross-equatorial winds and weak warming in the tropical South Atlantic appear soon after the tropical North Atlantic begins to cool, in support of interhemispheric air-sea interaction via wind-evaporation-SST feedback (Chiang and Bitz 2005; Chiang et al. 2008). The tropical Pacific response continues to intensify until year 50-60 except in ECHAM5-OM1, suggesting a slow oceanic adjustment process. There is some indication that

the North Pacific response intensifies concurrently with the tropical Pacific response.

The atmospheric circulation response in the North Pacific displays a distinct seasonal dependence, with a cyclonic circulation anomaly strongest in boreal winter and absent in summer (Fig. 3). An examination of the individual monthly responses shows that it typically appears in September-October and persists through March-April, the season when a semi-permanent low pressure center develops over the Aleutian Islands (not shown). Thus, the seasonal Aleutian Low becomes stronger when the AMOC slows down in the coupled GCMs. The extratropical atmospheric circulation anomalies are largest during the winter season not only in the North Pacific but also in the North Atlantic and the Southern Hemisphere (Fig. 3). The North Pacific cooling, in contrast, does not show much seasonality, with winter-to-summer differences less than 1°C. The tropical Atlantic and Pacific anomalies also exhibit some seasonal variations. The northeasterly winds across the Central American Isthmus are strongest in summer-early fall when the climatological ITCZ moves over the Caribbean Sea (Sutton and Hodson 2007; Xie et al. 2008). The zonal bands of precipitation anomalies move north and south following the seasonal migration of the ITCZ in both basins (not shown). The eastern Pacific precipitation anomalies become most asymmetric about the equator during winter.

#### **4. Atlantic-North Pacific teleconnection in CCSM2**

##### *a. Oceanic teleconnection through the Bering Strait*

The North Pacific is connected to the Arctic Ocean and ultimately, to the North Atlantic through the Bering Strait, a narrow and shallow pass between Alaska and Siberia. In present-day climate, the Bering Strait throughflow is hydraulically controlled and directed northward, transporting warmer and fresher water from the North Pacific into the Arctic Ocean (Woodgate et al. 2005). In the CCSM2 water-hosing experiment, part of the freshwater applied in the North

Atlantic flows into the Arctic Ocean, raising the sea level there and weakening the throughflow. The Bering Strait throughflow is eventually reversed after a decade and about 22% of the total added freshwater is discharged into the North Pacific by the end of the 100-year hosing period (Hu and Meehl 2005; Hu et al. 2007; Hu et al. 2008). Approximately 29% of this freshwater is transported as sea ice, increasing sea ice coverage along the Kamchatka Peninsula and in the Sea of Okhotsk by 30%-40% in the annual mean and 60%-70% in winter (not shown).

The reversal of the Bering Strait throughflow significantly impacts the heat and salinity balance in the North Pacific. Figure 4 shows the SST, precipitation, and sea-level pressure anomaly fields in the open and closed Bering Strait experiments and their differences averaged over the last 30 years of the hosing period for October-March, the season of the Aleutian Low response. When the Bering Strait is closed and no cold freshwater is transported from the Arctic Ocean, the magnitude of the North Pacific cooling is greatly reduced from  $-4^{\circ}\text{C}$  to  $-1^{\circ}\text{C}$ . In the difference map, which indicates the impact of the throughflow changes, negative SST anomalies extend from the eastern subarctic North Pacific to the west coast of the United States, and further into the subtropical basin. Associated with this subtropical cooling, the Pacific ITCZ shifts southward, contributing to more than half of the tropical Pacific precipitation changes in the open Bering Strait experiment. The Atlantic response is similar between the two experiments, although the magnitude of the northern cooling is reduced by  $1^{\circ}\text{C}$ - $2^{\circ}\text{C}$  in the open Bering Strait experiment due to faster removal of the freshwater anomaly and resultant weakening of the upper ocean stratification. It should be noted that the condition of the Bering Strait also affects the mean climates in the control runs (e.g., without freshwater forcing; not shown). When the Bering Strait is closed, the North Atlantic becomes slightly warmer and the North Pacific cools up to  $1^{\circ}\text{C}$ , with the Pacific ITCZ shifted southward. About one third of the response difference

between the two experiments (Fig. 4, bottom panel) arises from the difference in the control runs.

Contrary to the SST response, the wintertime Aleutian Low in the closed Bering Strait experiment is surprisingly similar to and even slightly stronger than that in the open Bering Strait experiment (Fig. 4). Geopotential height anomalies over this low pressure center display a quasi-barotropic structure with amplitudes increasing with height (Fig. 5, solid line). As in the open Bering Strait experiment, it appears only during the winter season when prevailing mean westerly winds enhance atmospheric teleconnections (cf. Fig. 12). The stronger North Pacific cooling in the open Bering Strait experiment compared to the closed one, on the other hand, induces a localized high pressure anomaly and thus weakens the Aleutian Low response (Fig. 4, bottom panel). The associated geopotential height anomaly difference between the open and closed Bering Strait experiments shows an out-of-phase relationship between the lower and upper troposphere (Fig. 5, dashed line), indicative of a direct baroclinic response to diabatic heating generated by local SST anomalies (Hoskins and Karoly 1981).

In the closed Bering Strait experiment, the rapid North Pacific cooling seen in all four coupled GCMs is absent and SST anomalies develop slowly during the first couple of decades (Fig. 6). Westerly wind anomalies are generally weaker in the closed Bering Strait experiment, especially in the band of  $50^{\circ}$ - $60^{\circ}$ N, due to the absence of a high pressure anomaly induced by strong North Pacific cooling (Fig. 4). The tropical Pacific precipitation anomalies appear at about the same time in the two experiments although they do not amplify after the third decade in the closed Bering Strait experiment unlike the open Bering Strait experiment (Fig. 6).

How does a change in the Bering Strait throughflow influence North Pacific SSTs in the open Bering Strait experiment? Figure 7 displays the time evolution of the SST and sea surface salinity anomaly fields from year 10 through 21. By the end of the first decade, the North Pacific

is already cooled by  $0.5^{\circ}$ - $1^{\circ}$ C. This cooling is likely due to the weakening of the Bering Strait throughflow and resultant reduction in the northward transport of heat and freshwater. In the closed Bering Strait experiment, in which atmospheric thermal advection and upward surface heat flux anomalies induced by atmospheric circulation changes are the major cause of North Pacific SST anomalies, basin-scale cooling does not occur until the second decade (not shown). Superimposed upon this overall cooling are large negative SST and salinity anomalies along the east coast of the Kamchatka Peninsula. During the second decade, the anomalies extend southeastward into the interior of the basin, following the mean ocean current shown in the bottom panel of Fig. 7. Upon reaching the west coast of the United States near the end of the second decade, the anomalies spread to the north and south along the coast with the southern branch penetrating into the subtropical basin. Thus, advection of temperature and salinity anomalies by the mean ocean current plays an important role for the rapid North Pacific cooling in the open Bering Strait experiment. The zonal ocean current averaged over  $35^{\circ}$ - $50^{\circ}$ N,  $140^{\circ}$ E- $120^{\circ}$ W and in the upper 100 m is  $4 \text{ cm s}^{-1}$ , giving the estimated time of 8.4 years to cross the basin, in agreement with the timescale inferred from the visual examination of SST and salinity anomaly fields. While the advection of cold water directly affects the mixed layer heat balance, the advection of freshwater indirectly contributes to the cooling by increasing the upper ocean stratification and reducing oceanic convection. To the best of our knowledge, this sensitivity of North Pacific SSTs to changes in the Bering Strait throughflow has not been described previously.

The importance of the Bering Strait throughflow for the North Pacific cooling may be model dependent. By the end of the 100-year hosing period, ECHAM5-OM1 and GFDL\_CM2.1 exhibit SST and sea surface salinity anomaly patterns very similar to Fig. 7 (see Fig. 4 of

Stouffer et al. 2007 for GFDL\_CM2.1). The Bering Strait throughflow is, indeed, reversed in the GFDL\_CM2.1 water-hosing experiment (J. Yin 2008, personal communication). Note that CCSM2 (GFDL\_CM2.1) is forced by virtual salt (real water) flux and thus the response of the Arctic sea level and the Bering Strait throughflow does not depend on the form of forcing. In HadCM3, on the other hand, negative salinity anomalies are mostly confined to the coastal region of the northwest Pacific and the strong SST cooling does not appear to be associated with the inflow of freshwater. Among the four coupled GCMs, CCSM2 displays the largest salinity anomalies over the North Pacific, suggesting that the Bering Strait throughflow may play a less important role in the other models.

In the open Bering Strait experiment, the surface turbulent (sensible plus latent) heat flux anomaly is downward over the region of maximum cooling in the North Pacific (the coast of Kamchatka Peninsula, the Sea of Okhotsk, and the oceanic frontal zone along 40°N; Fig. 8), confirming that this cooling is largely caused by oceanic processes. The maximum downward heat flux anomalies over the oceanic frontal zone are slightly displaced to the south of the maximum SST cooling due to the large westerly wind anomalies that cause upward turbulent heat fluxes between 50°-60°N. To the north of the oceanic frontal zone, these anomalous upward turbulent heat fluxes contribute to a cooling of the sea surface. The increased sea ice along the Kamchatka Peninsula and in the Sea of Okhotsk induces strong surface cooling and enhances the upward sensible heat flux to the east through atmospheric thermal advection. The enhanced westerly winds between 50°-60°N also cool the SSTs by increasing the southward Ekman heat transport although its impact is much weaker than the turbulent heat fluxes (Fig. 9). To the south of the oceanic frontal zone, upward turbulent heat flux anomalies are found in association with weak SST warming (Fig. 4), which is likely due to an anomalous northeastward oceanic current

in this region (not shown). In the closed Bering Strait experiment, the heat flux anomaly is in general negative and very small over the North Pacific, indicative of atmospheric forcing. Large negative values along the east coast of the Kamchatka Peninsula and northern Japan in this experiment are mostly attributable to sensible heat flux anomalies due to the outflow of anomalously cold continental air while wind-induced latent heat flux becomes more important in the interior basin (not shown). The stronger Aleutian Low response in the closed Bering Strait experiment (Fig. 4) also increases the southward Ekman transport, resulting in maximum cooling of  $-15 \text{ W m}^{-2}$  in the western basin (Fig. 9).

In both the open and closed Bering Strait experiments, the tropical North Pacific cooling is associated with enhanced trade winds (Fig. 6) and upward heat flux anomalies (Fig. 8); however, the wind and heat flux anomalies are twice as large in the open Bering Strait experiment compared to the closed one. The heat flux anomalies in this region are mostly due to wind-induced latent heat component with longwave and shortwave radiative fluxes nearly canceling each other (not shown). This suggests that the extratropical and subtropical cooling caused by oceanic advection intensifies the trade winds which in turn cool the tropical North Pacific by triggering wind-evaporation-SST feedback (Chiang and Bitz 2005; Wu et al. 2008). Off the Pacific coast of the Central American Isthmus, negative heat flux anomalies are of similar magnitude between the two experiments (Fig. 8), indicating that the North Atlantic cooling and resulting cross-Isthmus wind anomalies play a major role in cooling this region (Xie et al. 2008).

#### *b. Atmospheric teleconnection from the tropics*

What enhances the wintertime Aleutian Low when the AMOC slows down? SST and sea ice anomalies resulting from a weakening of the AMOC may affect the atmospheric circulation

over the North Pacific through several pathways, including the excitation of preferred circulation variability patterns and the propagation of Rossby waves remotely forced by tropical precipitation changes. We investigate these pathways by forcing CAM2 with regional SST and sea ice anomalies simulated in the *closed* Bering Strait experiment in which the Aleutian Low response is less influenced by local SSTs. Each experiment is integrated for 30 years.

When CAM2 is forced with the SST and sea ice anomalies in the entire Atlantic (25°S-75°N) and tropical Pacific (15°S-15°N) combined, the Aleutian Low deepens by 3 hPa during October-March, approximately 75% of the amplitude in the closed Bering Strait experiment and significant at the 98% level (Fig. 10, top left). The hemispheric pattern and vertical structure of geopotential height anomalies bear a close resemblance to those in the closed Bering Strait experiment (compare the first two columns in Fig. 11), indicating that the Atlantic and tropical Pacific together force a large part of the atmospheric circulation changes in the Northern Hemisphere. It is noted that the equivalent barotropic vertical structure of the geopotential height response is evident only over the North Pacific.

Which part of the remote forcing is important for the Aleutian Low response? SST and sea ice anomalies in the extratropical North Atlantic have been shown to drive a hemispheric annular mode response that resembles the leading internal mode of atmospheric circulation variability in an atmospheric GCM (Deser et al. 2004b; Magnúsdóttir et al. 2004), and Wu et al. (2008) explain the North Pacific wind anomalies associated with an AMOC shutdown by this mechanism. In CAM2 the SST cooling and sea ice increase in the extratropical North Atlantic (40°-75°N) raises sea-level pressure locally and downstream over Eurasia and the North Pacific (Fig. 10, lower right). Thus, the extratropical North Atlantic cooling is not a cause for the Aleutian Low response in the CCSM2 water-hosing experiments.

A southward shift of the Atlantic ITCZ is the most robust remote response to an AMOC weakening in both paleoclimate records and coupled GCMs (Chiang and Koutavas 2004; Stouffer et al. 2006). Large-scale shifts in tropical atmospheric convection can dramatically affect the global circulation as revealed by atmospheric teleconnection studies related to ENSO (Trenberth et al. 1998). When CAM2 is forced with the dipole pattern of SST anomalies in the tropical Atlantic (25°S-30°N), the Atlantic ITCZ is displaced to the south and sea-level pressure decreases by 2 hPa in the North Pacific with a barotropic structure in the vertical (significant at the 98% level; Fig. 10, lower left; Fig. 11, 4th column). Although the tropical and extratropical Atlantic SST anomalies have opposing impacts on North Pacific sea level pressure, CAM2's response to the entire Atlantic (25°S-75°N) SST anomaly pattern is dominated by the tropical Atlantic forcing (Fig. 10, upper right; Fig. 11, third column).

The tropical Atlantic SST anomalies explain about two thirds of the October-March Aleutian Low response to the full Atlantic plus tropical Pacific forcing (compare the two left panels in Fig. 10). The remaining one third is attributable to the tropical Pacific SST anomalies and the associated changes in atmospheric convection. These tropical Pacific SST anomalies are, in turn, forced by atmospheric teleconnection from the tropical Atlantic, implying a pivotal role of the tropical Atlantic in linking the AMOC and North Pacific climate. Previous studies of interannual and interdecadal Pacific variability show that a southward shift of the Pacific ITCZ and weakening of the Walker circulation act to strengthen the Aleutian Low by forcing barotropic Rossby waves and triggering the Pacific/North American pattern (Trenberth et al. 1998; Alexander et al. 2002; Deser and Phillips 2006), consistent with our results.

The relative importance of the tropical Atlantic and Pacific SST anomalies to the Aleutian Low response undergoes substantial changes from late fall through early spring (Fig.

12). Forced by the Atlantic and tropical Pacific SST anomalies, CAM2 simulates the monthly cycle of the Aleutian Low response in the closed Bering Strait experiment fairly well, confirming that these SST anomalies are responsible for the Aleutian Low response (compare gray and black lines in Fig. 12). The tropical Atlantic SSTs play a dominant role in late fall (October-November) and early spring (February-March; red line) while the tropical Pacific SSTs become more important in mid-winter (December-January; green line). This seasonal sensitivity of the Aleutian Low to tropical Pacific SSTs is in agreement with studies of ENSO teleconnections (Alexander et al. 2002). The extratropical North Atlantic cooling, on the other hand, damps the Aleutian Low response during winter when the annular mode variability becomes most vigorous (Thompson and Wallace 2000).

The consistency of the Aleutian Low response among the four coupled GCMs suggests that similar teleconnection mechanisms are at work in the other models. The relative importance of each remote forcing mechanism, however, may be model-dependent due to differences in the models' mean climate. For example, in the tropical Atlantic, most coupled GCMs fail to simulate the eastern equatorial cold tongue, resulting in an ITCZ that is displaced too far south compared to observations (Davey et al. 2002; Richter and Xie 2008). This tropical Atlantic bias is prominent in CCSM2 (Fig. 13). The Caribbean warm pool is also absent and the mean precipitation is less than  $2 \text{ mm day}^{-1}$  in the western tropical North Atlantic, where a strong cooling occurs in response to an AMOC weakening. With the mean SST too low to sustain deep atmospheric convection, further SST cooling does not significantly impact the atmospheric convection and hence the resultant forcing of barotropic Rossby waves. To test this hypothesis, we repeated the CAM2 tropical Atlantic experiment by replacing the mean SST and sea ice fields with observed climatologies from the HadISST data set for the period 1949-2001 (Rayner

et al. 2003). In response to the same tropical Atlantic SST forcing, replacing the climatology with observations results in a doubling of the precipitation anomalies in the tropical North Atlantic and tripling of the Aleutian Low response (compare Fig. 14 to the lower left panel of Fig. 10). The precipitation anomalies in the tropical South Atlantic, on the other hand, weaken significantly and the southward shift of the Atlantic ITCZ becomes inconspicuous. CCSM2 is one of the models with the most severe tropical Atlantic bias (see Fig. 1 in Timmermann et al. 2007) and its tropical North Atlantic precipitation anomalies in the water-hosing experiment are smallest among the four coupled GCMs (Fig. 1). Therefore, it is plausible that the atmospheric bridge from the tropical North Atlantic to the North Pacific is stronger in the other three models and also in the real world during the last glacial period compared to CCSM2.

Using the atmospheric GCM component of HadCM3, Sutton and Hodson (2007) examined the relative importance of tropical and extratropical Atlantic SST anomalies for the atmospheric circulation changes associated with the Atlantic multidecadal oscillation which exhibits anomaly patterns similar to those in the water-hosing experiment. The tropical Atlantic SST anomalies explain a large part of the Aleutian Low change in this model (compare their Figs. 3 and 4), consistent with our result. On the other hand, Zhang et al. (2007) find that extratropical North Atlantic SST anomalies are more important than tropical Atlantic ones for the North Pacific climate response associated with the Atlantic multidecadal oscillation using the atmospheric GCM of GFDL\_CM2.1. In their experiment, however, the atmospheric GCM is coupled to a slab ocean model globally and the heating anomaly prescribed in the extratropical North Atlantic induces significant SST changes in the tropical North Atlantic *via* atmospheric teleconnections, making it difficult to isolate the relative importance of tropical and extratropical Atlantic SST anomalies.

## 5. Summary and discussion

The analysis of water-hosing experiments with four coupled GCMs revealed a strong linkage between the AMOC and North Pacific climate, consistent with paleoclimate reconstructions. When the AMOC is forced to slow down in the models, strong cooling occurs along the North Pacific oceanic frontal zone and the wintertime Aleutian Low intensifies. This remote response establishes quickly within a few decades. Through additional experiments with CCSM2 and CAM2, mechanisms for both oceanic and atmospheric teleconnections are proposed. For the oceanic teleconnection, part of the freshwater applied to the North Atlantic flows through the Bering Strait into the North Pacific, where the anomalously cold and fresh water is advected by mean ocean currents. The resulting extratropical oceanic cooling strengthens the northeasterly trade winds, reducing the tropical North Pacific SSTs and shifting the Pacific ITCZ southward through the wind-evaporation-SST feedback. For the atmospheric teleconnection, precipitation changes associated with the tropical Atlantic and Pacific SST anomalies force barotropic Rossby waves, inducing a cyclonic circulation anomaly over the North Pacific from late fall through early spring. The enhanced Aleutian Low, in turn, cools the oceanic frontal zone by increasing surface heat losses and southward Ekman transport, although this cooling is considerably weaker than that due to the Bering Strait throughflow change. The tropical North Atlantic is a particularly important region for this atmospheric bridge since it influences the atmospheric circulation in the North Pacific not only directly but also indirectly by triggering SST and precipitation changes in the eastern tropical Pacific. In the tropical North Atlantic, the excitation of atmospheric Rossby waves is quite sensitive to the background SST and precipitation distributions, which are underestimated in most coupled GCMs.

The response of the Aleutian Low to tropical Atlantic SSTs cannot be readily explained

and will require further investigation. A preliminary analysis, however, suggests that the upper tropospheric convergence associated with the suppressed precipitation in the tropical North Atlantic forces barotropic Rossby waves that propagate along the South Asian westerly jet and then into the North Pacific (not shown). Near the entrance of the South Asian waveguide, where the energy dispersion is small and the group velocity is exceptionally large (Hoskins and Ambrizzi 1993; Branstator 2002), atmospheric convection changes in the tropical North Atlantic can exert a significant impact on the North Pacific atmospheric circulation. Haarsma and Hazeleger (2007) show that atmospheric Rossby waves forced by equatorial Atlantic SST anomalies propagate circumglobally through the South Asian waveguide in a matter of two weeks in their model. A Japanese community atmospheric GCM forced with an idealized tropical Atlantic SST dipole (Okumura et al. 2001) also obtains a deepening of the wintertime Aleutian Low when atmospheric convection is suppressed in the tropical North Atlantic. In addition to Rossby wave propagation, the structure of intrinsic circulation variability may also play an important role in shaping the anomaly pattern over the North Pacific. The Aleutian Low response in both the open and closed Bering Strait experiments projects onto the second leading mode of North Pacific variability in the control simulations which resembles the Pacific/North American pattern (Wallace and Gutzler 1981; not shown).

During the last glacial period when the Bering Strait was closed, the atmospheric teleconnection from the tropical Atlantic and Pacific is likely to have played a fundamental role in the AMOC-North Pacific teleconnection. In the closed Bering Strait experiment, however, the North Pacific cools only by 1°C, much smaller than the magnitude of 3°-6°C inferred from paleoclimate records (Thunell and Mortyn 1995; Hendy and Kennett 1999; Kienast and McKay 2001). The weaker atmospheric bridge from the tropical North Atlantic due to model errors may

partly contribute to this gap. With the mean Atlantic ITCZ displaced north of the equator, the tropical North Atlantic cooling induces a stronger Aleutian Low response that enhances the SST cooling by increasing surface heat fluxes and southward Ekman transport, and shifting the subarctic gyre to the south. Despite the absence of freshwater exchange with the Arctic Ocean through the Bering Strait, Kotilainen and Shackleton (1995) report rapid variability in ice-rafted detritus in the subarctic North Pacific Ocean sediment cores associated with the Greenland ice core records. During cold phases in Greenland, increased discharge of icebergs might have freshened the upper ocean and contributed to the surface cooling by inhibiting oceanic convection.

Another important issue not explored in this study is the role of sea ice and its interaction with the ocean and atmosphere. Cheng et al. (2007) compare two sets of water-hosing experiments under different background states for the present day and Last Glacial Maximum—the time of maximum extent of the ice sheets during the last glacial (~20 kyr ago). They find that the fundamental mechanisms for global adjustment to an AMOC weakening are similar between the two experiments. However, under the Last Glacial Maximum condition, the climatic impact is much more severe than that under the present-day condition primarily due to the more extensive distribution of sea ice and stronger ice-albedo feedback. In our CCSM2 experiments, the closure of the Bering Strait alone only modestly enhances the mean sea ice distribution in the Sea of Okhotsk, and sea ice concentration anomalies in the water-hosing experiment are less than 10% over the subarctic North Pacific (not shown). The presence of continental ice sheets and their interaction with the overlying atmosphere may have had a more profound impact on the North Pacific sea ice distribution during the Last Glacial Maximum than the closure of the Bering Strait. Sea ice, if presents, acts as an insulator between the ocean and atmosphere,

reducing the thermal damping of anomalously cold outflow from the Eurasian continent and thus amplifying the North Pacific cooling. The results of Cheng et al. (2007) and our analysis of the oceanic teleconnection via the Bering Strait point to the importance of background states in determining the climate response to freshwater perturbations in the North Atlantic.

Our analysis of coupled and atmospheric GCM experiments offers a framework for interpreting abrupt climate shifts in the North Pacific and their relation to changes in the AMOC in paleoclimate records beyond the thermal advection mechanism. Furthermore, it has significant implications for present-day and future climate. Concern about future climate change induced by increasing greenhouse gases partly stems from the possibility that Arctic warming and rapid melting of continental/sea ice may halt the AMOC, leading to a drastic transition of global climate (Manabe and Stouffer 1993; Stocker and Schmittner 1997). Although the current generation of coupled GCMs suggests that such an extreme scenario is unlikely, most models do predict a gradual weakening of the AMOC in response to an increase in greenhouse gases (Gregory et al. 2005; Meehl et al. 2007). Superimposed on an overall greenhouse warming, the weakening AMOC may influence climate over the North Pacific and other distant regions according to the pathways described in this study. Indeed, the North Pacific displays a cooling trend over the recent 50 years associated with a cooling (warming) trend in the North (South) Atlantic that is possibly caused by a weakening of the AMOC (Trenberth et al. 2006). This SST anomaly pattern may also reflect Atlantic multidecadal oscillation which involves modulation of the AMOC intensity (Timmermann et al. 1998; Enfield and Mestas-Nunez 1999; Delworth and Mann 2000; Knight et al. 2005; Sutton and Hodson 2005). Based on analyses of reconstructed surface temperature data and coupled GCM simulations, these studies show that the Atlantic multidecadal oscillation yields a hemispheric anomaly pattern with a significant SST change in

the extratropical North Pacific that is nearly in phase with the SST change in the North Atlantic. Atmospheric teleconnections from the Atlantic can be responsible for the Pacific portion of this inter-basin multidecadal variability (Timmermann et al. 1998; Enfield and Mestas-Nunez 1999; Sutton and Hodson 2007; Zhang and Delworth 2007). Zhang and Delworth (2007) show that the Aleutian Low change forced from the Atlantic induces SST anomalies in the oceanic frontal region with a lag of several years in GFDL\_CM2.1, suggesting the transient adjustment of the gyre-scale circulation to a change in wind stress curl *via* long baroclinic Rossby waves (e.g., Miller et al. 1998; Deser et al. 1999). Under present-day boundary conditions, the oceanic teleconnection via the Bering Strait may also come into play. This inter-basin oceanic adjustment is suggested to stabilize the AMOC, hence present-day, interglacial climate (De Boer and Nof 2004; Hu et al. 2007). While it remains to be seen whether the AMOC-North Pacific teleconnection mechanisms described in this study operate in association with the anthropogenic change and multidecadal variability of the AMOC, they potentially offer wide-ranging applications to Atlantic and Pacific climate variability on long time scales.

***Acknowledgements.*** The authors are grateful to J. Jungclaus, J. Yin, and B. Dong for providing the CMIP/PMIP water-hosing experiment data from ECHAM5-OM1, GFDL\_CM2.1, and HadCM3. Discussions with Y.-O. Kwon and J. M. Wallace helped refine the analysis and its physical interpretation. We thank the anonymous reviewers for their useful suggestions. Y. Okumura is supported by the NOAA Climate and Global Change Postdoctoral Fellowship. A. Timmermann and S.-P. Xie acknowledge support from the Japan Agency for Marine-Earth Science and technology (JAMSTEC), NASA through grant No. NNX07AG53G, and NOAA through grant No. NA17RJ1230. A. Timmermann is also supported by NSF grant No. ATM06-

28393. This study was in part supported by the Office of Science (BER), U.S. Department of Energy, Cooperative Agreement No. DE-FC02-97ER62402. The CAM2 simulations were conducted using computational resources from the NCAR Director's Reserve.

## References

- Alexander, M. A., I. Blade, M. Newman, J. R. Lanzante, N. C. Lau, and J. D. Scott, 2002: The atmospheric bridge: The influence of ENSO teleconnections on air-sea interaction over the global oceans. *J. Climate*, **15**, 2205-2231.
- Altabet, M. A., M. J. Higginson, and D. W. Murray, 2002: The effect of millennial-scale changes in Arabian Sea denitrification on atmospheric CO<sub>2</sub>. *Nature*, **415**, 159-162.
- Behl, R. J., and J. P. Kennett, 1996: Brief interstadial events in the Santa Barbara basin, NE Pacific, during the past 60 kyr. *Nature*, **379**, 243-246.
- Bond, G. C., and R. Lotti, 1995: Iceberg discharges into the North Atlantic on millennial time scales during the last glaciation. *Science*, **267**, 1005-1010.
- Boyle, E. A., and L. Keigwin, 1987: North Atlantic thermohaline circulation during the past 20,000 years linked to high-latitude surface temperature. *Nature*, **330**, 35-40.
- Branstator, G., 2002: Circumglobal teleconnections, the jet stream waveguide, and the North Atlantic oscillation. *J. Climate*, **15**, 1893-1910.
- Broecker, W. S., D. M. Peteet, and D. Rind, 1985: Does the ocean-atmosphere system have more than one stable mode of operation? *Nature*, **315**, 21-26.
- Bryan, F., 1986: High-latitude salinity effects and interhemispheric thermohaline circulations. *Nature*, **323**, 301-304.
- Chappell, J., 2002: Sea level changes forced ice breakouts in the last glacial cycle: new results from coral terraces. *Quaternary Science Reviews*, **21**, 1229-1240.
- Cheng, W., C. M. Bitz, and J. C. H. Chiang, 2007: Adjustment of the global climate to an abrupt slowdown of the Atlantic meridional overturning circulation. *Ocean circulation: Mechanisms and impacts*, *Geophys. Monogr.*, No. 173, Amer. Geophys. Union, 295-314.

- Chiang, J. C. H., and A. Koutavas, 2004: Climate change - Tropical flip-flop connections. *Nature*, **432**, 684-685.
- Chiang, J. C. H., and C. M. Bitz, 2005: Influence of high latitude ice cover on the marine intertropical convergence zone. *Climate Dyn.*, **25**, 477-496.
- Chiang, J. C. H., W. Cheng, and C. M. Bitz, 2008: Fast teleconnections to the tropical Atlantic sector from Atlantic thermohaline adjustment. *Geophys. Res. Lett.*, **35**, L07704, doi:10.1029/2008GL033292.
- Clark, P. U., A. M. McCabe, A. C. Mix, and A. J. Weaver, 2004: Rapid rise of sea level 19,000 years ago and its global implications. *Science*, **304**, 1141-1144.
- Clarke, G., D. Leverington, J. Teller, and A. Dyke, 2003: Superlakes, megafloods, and abrupt climate change. *Science*, **301**, 922-923.
- Dansgaard, W., and Coauthors, 1993: Evidence for general instability of past climate from a 250-kyr ice core record. *Nature*, **364**, 218-220.
- Davey, M. K., and Coauthors, 2002: STOIC: A study of coupled model climatology and variability in tropical ocean regions. *Climate Dyn.*, **18**, 403-420.
- De Boer, A. M., and D. Nof, 2004: The Bering Strait is grip on the Northern Hemisphere climate. *Deep-Sea Res.*, **51**, 1347-1366.
- Delworth, T. L., and M. E. Mann, 2000: Observed and simulated multidecadal variability in the Northern Hemisphere. *Climate Dyn.*, **16**, 661-676.
- Delworth, T. L., and Coauthors, 2006: GFDL's CM2 global coupled climate models. Part I: Formulation and simulation characteristics. *J. Climate*, **19**, 643-674.
- Deser, C., and A. S. Phillips, 2006: Simulation of the 1976/77 climate transition over the North Pacific: Sensitivity to tropical forcing. *J. Climate*, **19**, 6170-6180.

- Deser, C., M. A. Alexander, and M. S. Timlin, 1999: Evidence for a wind-driven intensification of the Kuroshio Current extension from the 1970s to the 1980s. *J. Climate*, **12**, 1697-1706.
- Deser, C., A. S. Phillips, and J. W. Hurrell, 2004a: Pacific interdecadal climate variability: Linkages between the tropics and the North Pacific during boreal winter since 1900. *J. Climate*, **17**, 3109-3124.
- Deser, C., G. Magnusdottir, R. Saravanan, and A. Phillips, 2004b: The effects of North Atlantic SST and sea ice anomalies on the winter circulation in CCM3. Part II: Direct and indirect components of the response. *J. Climate*, **17**, 877-889.
- Dong, B. W., and R. T. Sutton, 2002: Adjustment of the coupled ocean-atmosphere system to a sudden change in the thermohaline circulation. *Geophys. Res. Lett.*, **29**, 1728, doi:10.1029/2002GL015229.
- Enfield, D. B., and A. M. Mestas-Nunez, 1999: Multiscale variabilities in global sea surface temperatures and their relationships with tropospheric climate patterns. *J. Climate*, **12**, 2719-2733.
- Gordon, C., C. Cooper, C. A. Senior, H. Banks, J. M. Gregory, T. C. Johns, J. F. B. Mitchell, and R. A. Wood, 2000: The simulation of SST, sea ice extents and ocean heat transports in a version of the Hadley Centre coupled model without flux adjustments. *Climate Dyn.*, **16**, 147-168.
- Gregory, J. M., and Coauthors, 2005: A model intercomparison of changes in the Atlantic thermohaline circulation in response to increasing atmospheric CO<sub>2</sub> concentration. *Geophys. Res. Lett.*, **32**, L12703, doi:10.1029/2005GL023209.
- Haarsma, R. J., and W. Hazeleger, 2007: Extratropical atmospheric response to equatorial Atlantic cold tongue anomalies. *J. Climate*, **20**, 2076-2091.

- Harada, N., N. Ahagon, T. Sakamoto, M. Uchida, M. Ikehara, and Y. Shibata, 2006: Rapid fluctuation of alkenone temperature in the southwestern Okhotsk Sea during the past 120 ky. *Global Planet. Change*, **53**, 29-46.
- Heinrich, H., 1988: Origin and consequences of cyclic ice rafting in the northeast Atlantic Ocean during the past 130,000 years. *Quatern. Res.*, **29**, 142-152.
- Hendy, I. L., and J. P. Kennett, 1999: Latest Quaternary North Pacific surface-water responses imply atmosphere-driven climate instability. *Geology*, **27**, 291-294.
- Hoskins, B. J., and D. J. Karoly, 1981: The steady linear response of a spherical atmosphere to thermal and orographic forcing. *J. Atmos. Sci.*, **38**, 1179-1196.
- Hoskins, B. J., and T. Ambrizzi, 1993: Rossby wave propagation on a realistic longitudinally varying flow. *J. Atmos. Sci.*, **50**, 1661-1671.
- Hu, A., and G. A. Meehl, 2005: Bering Strait throughflow and the thermohaline circulation. *Geophys. Res. Lett.*, **32**, L24610, doi:10.1029/2005GL024424.
- Hu, A., G. A. Meehl, and W. Q. Han, 2007: Role of the Bering Strait in the thermohaline circulation and abrupt climate change. *Geophys. Res. Lett.*, **34**, L05704, doi:10.1029/2006GL028906.
- Hu, A., B. L. Otto-Bliesner, G. A. Meehl, W. Q. Han, C. Morrill, E. C. Brady, and B. Briegleb, 2008: Response of thermohaline circulation to freshwater forcing under present-day and LGM conditions. *J. Climate*, **21**, 2239-2258.
- Hu, F. S., D. M. Nelson, G. H. Clarke, K. M. Ruhland, Y. S. Huang, D. S. Kaufman, and J. P. Smol, 2006: Abrupt climatic events during the last glacial-interglacial transition in Alaska. *Geophys. Res. Lett.*, **33**, L18708, doi:10.1029/2006GL027261.

- Ivanochko, T. S., R. S. Ganeshram, G. J. A. Brummer, G. Ganssen, S. J. A. Jung, S. G. Moreton, and D. Kroon, 2005: Variations in tropical convection as an amplifier of global climate change at the millennial scale. *Earth Planet. Sci. Lett.*, **235**, 302-314.
- Jungclauss, J. H., and Coauthors, 2006: Ocean circulation and tropical variability in the coupled model ECHAM5/MPI-OM. *J. Climate*, **19**, 3952-3972.
- Kiefer, T., M. Sarnthein, H. Erlenkeuser, P. M. Grootes, and A. P. Roberts, 2001: North Pacific response to millennial-scale changes in ocean circulation over the last 60 kyr. *Paleoceanography*, **16**, 179-189.
- Kiehl, J. T., and P. R. Gent, 2004: The Community Climate System Model, version 2. *J. Climate*, **17**, 3666-3682.
- Kienast, S. S., and J. L. McKay, 2001: Sea surface temperatures in the subarctic Northeast Pacific reflect millennial-scale climate oscillations during the last 16 kyrs. *Geophys. Res. Lett.*, **28**, 1563-1566.
- Kienast, M., S. S. Kienast, S. E. Calvert, T. I. Eglinton, G. Mollenhauer, R. Francois, and A. C. Mix, 2006: Eastern Pacific cooling and Atlantic overturning circulation during the last deglaciation. *Nature*, **443**, 846-849.
- Knight, J. R., R. J. Allan, C. K. Folland, M. Vellinga, and M. E. Mann, 2005: A signature of persistent natural thermohaline circulation cycles in observed climate. *Geophys. Res. Lett.*, **32**, L20708, doi:10.1029/2005GL024233.
- Knutti, R., J. Fluckiger, T. F. Stocker, and A. Timmermann, 2004: Strong hemispheric coupling of glacial climate through freshwater discharge and ocean circulation. *Nature*, **430**, 851-856.
- Kotilainen, A. T., and N. J. Shackleton, 1995: Rapid climate variability in the North Pacific Ocean during the past 95,000 years. *Nature*, **377**, 323-326.

- Koutavas, A., J. Lynch-Stieglitz, T. M. Marchitto, and J. P. Sachs, 2002: El Nino-like pattern in ice age tropical Pacific sea surface temperature. *Science*, **297**, 226-230.
- Krebs, U., and A. Timmermann, 2007: Tropical air-sea interactions accelerate the recovery of the Atlantic meridional overturning circulation after a major shutdown. *J. Climate*, **20**, 4940-4956.
- Leduc, G., L. Vidal, K. Tachikawa, F. Rostek, C. Sonzogni, L. Beaufort, and E. Bard, 2007: Moisture transport across Central America as a positive feedback on abrupt climatic changes. *Nature*, **445**, 908-911.
- Lund, D. C., and A. C. Mix, 1998: Millennial-scale deep water oscillations: Reflections of the North Atlantic in the deep Pacific from 10 to 60 ka. *Paleoceanography*, **13**, 10-19.
- Magnusdottir, G., C. Deser, and R. Saravanan, 2004: The effects of North Atlantic SST and sea ice anomalies on the winter circulation in CCM3. Part I: Main features and storm track characteristics of the response. *J. Climate*, **17**, 857-876.
- Manabe, S., and R. J. Stouffer, 1988: Two stable equilibria of a coupled ocean-atmosphere model. *J. Climate*, **1**, 841-866.
- Manabe, S., and R. J. Stouffer, 1993: Century-scale effects of increased atmospheric CO<sub>2</sub> on the ocean-atmosphere system. *Nature*, **364**, 215-218.
- Manabe, S., and R. J. Stouffer, 1997: Coupled ocean-atmosphere model response to freshwater input: Comparison to Younger Dryas event. *Paleoceanography*, **12**, 321-336.
- Mantua, N. J., S. R. Hare, Y. Zhang, J. M. Wallace, and R. C. Francis, 1997: A Pacific interdecadal climate oscillation with impacts on salmon production. *Bull. Amer. Meteor. Soc.*, **78**, 1069-1079.

- McManus, J. F., R. Francois, J. M. Gherardi, L. D. Keigwin, and S. Brown-Leger, 2004: Collapse and rapid resumption of Atlantic meridional circulation linked to deglacial climate changes. *Nature*, **428**, 834-837.
- Meehl, G. A., and Coauthors, 2007: Global climate projections. *Climate change 2007: The physical science basis*, S. Solomon, D. Qin, M. Manning, Z. Chen, M. Marquis, K. B. Averyt, M. Tignor and H. L. Miller eds., Cambridge University Press Kingdom, 747-846.
- Mikolajewicz, U., and E. Maier-Reimer, 1994: Mixed boundary conditions in ocean general circulation models and their influence on the stability of the models' conveyor belt. *J. Geophys. Res.*, **99**, 22633-22644.
- Mikolajewicz, U., T. J. Crowley, A. Schiller, and R. Voss, 1997: Modelling teleconnections between the North Atlantic and North Pacific during the Younger Dryas. *Nature*, **387**, 384-387.
- Mikolajewicz, U., M. Groger, E. Maier-Reimer, G. Schurgers, M. Vizcaino, and A. M. E. Winguth, 2007: Long-term effects of anthropogenic CO<sub>2</sub> emissions simulated with a complex earth system model. *Climate Dyn.*, **28**, 599-631.
- Miller, A. J., D. R. Cayan, and W. B. White, 1998: A westward-intensified decadal change in the North Pacific thermocline and gyre-scale circulation. *J. Climate*, **11**, 3112-3127.
- Okumura, Y., S. P. Xie, A. Numaguti, and Y. Tanimoto, 2001: Tropical Atlantic air-sea interaction and its influence on the NAO. *Geophys. Res. Lett.*, **28**, 1507-1510.
- Oppo, D. W., and S. J. Lehman, 1995: Suborbital timescale variability of North Atlantic deep water during the past 200,000 years. *Paleoceanography*, **10**, 901-910.
- Peterson, L. C., G. H. Haug, K. A. Hughen, and U. Rohl, 2000: Rapid changes in the hydrologic cycle of the tropical Atlantic during the last glacial. *Science*, **290**, 1947-1951.

- Rahmstorf, S., 1995: Bifurcations of the Atlantic thermohaline circulation in response to changes in the hydrological cycle. *Nature*, **378**, 145-149.
- Rayner, N. A., D. E. Parker, E. B. Horton, C. K. Folland, L. V. Alexander, D. P. Rowell, E. C. Kent, and A. Kaplan, 2003: Global analyses of sea surface temperature, sea ice, and night marine air temperature since the late nineteenth century. *J. Geophys. Res.*, **108**, 4407, doi:10.1029/2002JD002670.
- Reichler, T., and J. Kim, 2008: How well do coupled models simulate today's climate? *Bull. Amer. Meteor. Soc.*, **89**, 303-311.
- Richter, I., and S. P. Xie, 2008: On the origin of equatorial Atlantic biases in coupled general circulation models. *Climate Dyn.*, in press.
- Rooth, C., 1982: Hydrology and ocean circulation. *Prog. Oceanogr.*, **11**, 131-149.
- Saenko, O. A., A. Schmittner, and A. J. Weaver, 2004: The Atlantic-Pacific seesaw. *J. Climate*, **17**, 2033-2038.
- Saenko, O. A., A. J. Weaver, D. Y. Robitaille, and G. M. Flato, 2007: Warming of the subpolar Atlantic triggered by freshwater discharge at the continental boundary. *Geophys. Res. Lett.*, **34**, L15604, doi:10.1029/2007GL030674.
- Sarnthein, M., T. Kiefer, P. M. Grootes, H. Elderfield, and H. Erlenkeuser, 2006: Warmings in the far northwestern Pacific promoted pre-Clovis immigration to America during Heinrich event 1. *Geology*, **34**, 141-144.
- Schiller, A., U. Mikolajewicz, and R. Voss, 1997: The stability of the North Atlantic thermohaline circulation in a coupled ocean-atmosphere general circulation model. *Climate Dyn.*, **13**, 325-347.

- Schmidt, M. W., M. J. Vautravers, and H. J. Spero, 2006: Rapid subtropical North Atlantic salinity oscillations across Dansgaard-Oeschger cycles. *Nature*, **443**, 561-564.
- Siddall, M., E. J. Rohling, A. Almogi-Labin, C. Hemleben, D. Meischner, I. Schmelzer, and D. A. Smeed, 2003: Sea-level fluctuations during the last glacial cycle. *Nature*, **423**, 853-858.
- Stocker, T. F., and A. Schmittner, 1997: Influence of CO<sub>2</sub> emission rates on the stability of the thermohaline circulation. *Nature*, **388**, 862-865.
- Stommel, H., 1961: Thermohaline convection with two stable regimes of flow. *Tellus*, **13**, 224-230.
- Stott, L., C. Poulsen, S. Lund, and R. Thunell, 2002: Super ENSO and global climate oscillations at millennial time scales. *Science*, **297**, 222-226.
- Stouffer, R. J., and Coauthors, 2006: Investigating the causes of the response of the thermohaline circulation to past and future climate changes. *J. Climate*, **19**, 1365-1387.
- Stouffer, R. J., D. Seidov, and B. J. Haupt, 2007: Climate response to external sources of freshwater: North Atlantic versus the Southern Ocean. *J. Climate*, **20**, 436-448.
- Sutton, R. T., and D. L. R. Hodson, 2005: Atlantic Ocean forcing of North American and European summer climate. *Science*, **309**, 115-118.
- Sutton, R. T., and D. L. R. Hodson, 2007: Climate response to basin-scale warming and cooling of the North Atlantic Ocean. *J. Climate*, **20**, 891-907.
- Thompson, D. W. J., and J. M. Wallace, 2000: Annular modes in the extratropical circulation. Part I: Month-to-month variability. *J. Climate*, **13**, 1000-1016.
- Thunell, R. C., and P. G. Mortyn, 1995: Glacial climate instability in the northeast Pacific Ocean. *Nature*, **376**, 504-506.

- Timmermann, A., M. Latif, R. Voss, and A. Grotzner, 1998: Northern Hemispheric interdecadal variability: A coupled air-sea mode. *J. Climate*, **11**, 1906-1931.
- Timmermann, A., S. I. An, U. Krebs, and H. Goosse, 2005a: ENSO suppression due to weakening of the North Atlantic thermohaline circulation. *J. Climate*, **18**, 3122-3139.
- Timmermann, A., U. Krebs, F. Justino, H. Goosse, and T. Ivanochko, 2005b: Mechanisms for millennial-scale global synchronization during the last glacial period. *Paleoceanography*, **20**, 19.
- Timmermann, A., and Coauthors, 2007: The influence of a weakening of the Atlantic meridional overturning circulation on ENSO. *J. Climate*, **20**, 4899-4919.
- Trenberth, K. E., and J. W. Hurrell, 1994: Decadal atmosphere-ocean variations in the Pacific. *Climate Dyn.*, **9**, 303-319.
- Trenberth, K. E., G. W. Branstator, D. Karoly, A. Kumar, N. C. Lau, and C. Ropelewski, 1998: Progress during TOGA in understanding and modeling global teleconnections associated with tropical sea surface temperatures. *J. Geophys. Res.*, **103**, 14291-14324.
- Trenberth, K. E., B. Moore, T. R. Karl, and C. Nobre, 2006: Monitoring and prediction of the earth's climate: A future perspective. *J. Climate*, **19**, 5001-5008.
- Vellinga, M., and R. A. Wood, 2002: Global climatic impacts of a collapse of the Atlantic thermohaline circulation. *Climate Change*, **54**, 251-267.
- Wallace, J. M., and D. S. Gutzler, 1981: Teleconnections in the geopotential height field during the Northern Hemisphere winter. *Mon. Wea. Rev.*, **109**, 784-812.
- Wang, X. F., A. S. Auler, R. L. Edwards, H. Cheng, P. S. Cristalli, P. L. Smart, D. A. Richards, and C. C. Shen, 2004: Wet periods in northeastern Brazil over the past 210 kyr linked to distant climate anomalies. *Nature*, **432**, 740-743.

- Wang, Y. J., H. Cheng, R. L. Edwards, Z. S. An, J. Y. Wu, C. C. Shen, and J. A. Dorale, 2001: A high-resolution absolute-dated Late Pleistocene monsoon record from Hulu Cave, China. *Science*, **294**, 2345-2348.
- Weart, S., 2003: The discovery of rapid climate change. *Phys Today*, **56**, 30-36.
- Woodgate, R. A., K. Aagaard, and T. J. Weingartner, 2005: Monthly temperature, salinity, and transport variability of the Bering Strait through flow. *Geophys. Res. Lett.*, **32**, L04601, doi:10.1029/2004GL021880.
- Wu, L., C. Li, C. Yang, and S. P. Xie, 2008: Global teleconnections in response to a shutdown of the Atlantic meridional overturning circulation. *J. Climate*, in press.
- Xie, S. P., and J. A. Carton, 2004: Tropical Atlantic variability: Patterns, mechanisms, and impacts. *Earth's Climate: The Ocean-Atmosphere Interaction, Geophys. Monogr.*, No. 147, Amer. Geophys. Union, 121-142.
- Xie, S. P., Y. Okumura, T. Miyama, and A. Timmermann, 2008: Influences of Atlantic climate change on the tropical Pacific via the Central American Isthmus. *J. Climate*, **21**, 3914-3928.
- Yang, J. Y., 1999: A linkage between decadal climate variations in the Labrador Sea and the tropical Atlantic Ocean. *Geophys. Res. Lett.*, **26**, 1023-1026.
- Yin, J., and R. J. Stouffer, 2007: Comparison of the stability of the Atlantic thermohaline circulation in two coupled atmosphere-ocean general circulation models. *J. Climate*, **20**, 4293-4315.
- Zhang, R., and T. L. Delworth, 2005: Simulated tropical response to a substantial weakening of the Atlantic thermohaline circulation. *J. Climate*, **18**, 1853-1860.
- Zhang, R., and T. L. Delworth, 2007: Impact of the Atlantic multidecadal oscillation on North Pacific climate variability. *Geophys. Res. Lett.*, **34**, L23708, doi:10.1029/2007GL031601.

Zhang, R., T. L. Delworth, and I. M. Held, 2007: Can the Atlantic Ocean drive the observed multidecadal variability in Northern Hemisphere mean temperature? *Geophys. Res. Lett.*, **34**, L02709, doi:10.1029/2006GL028683.

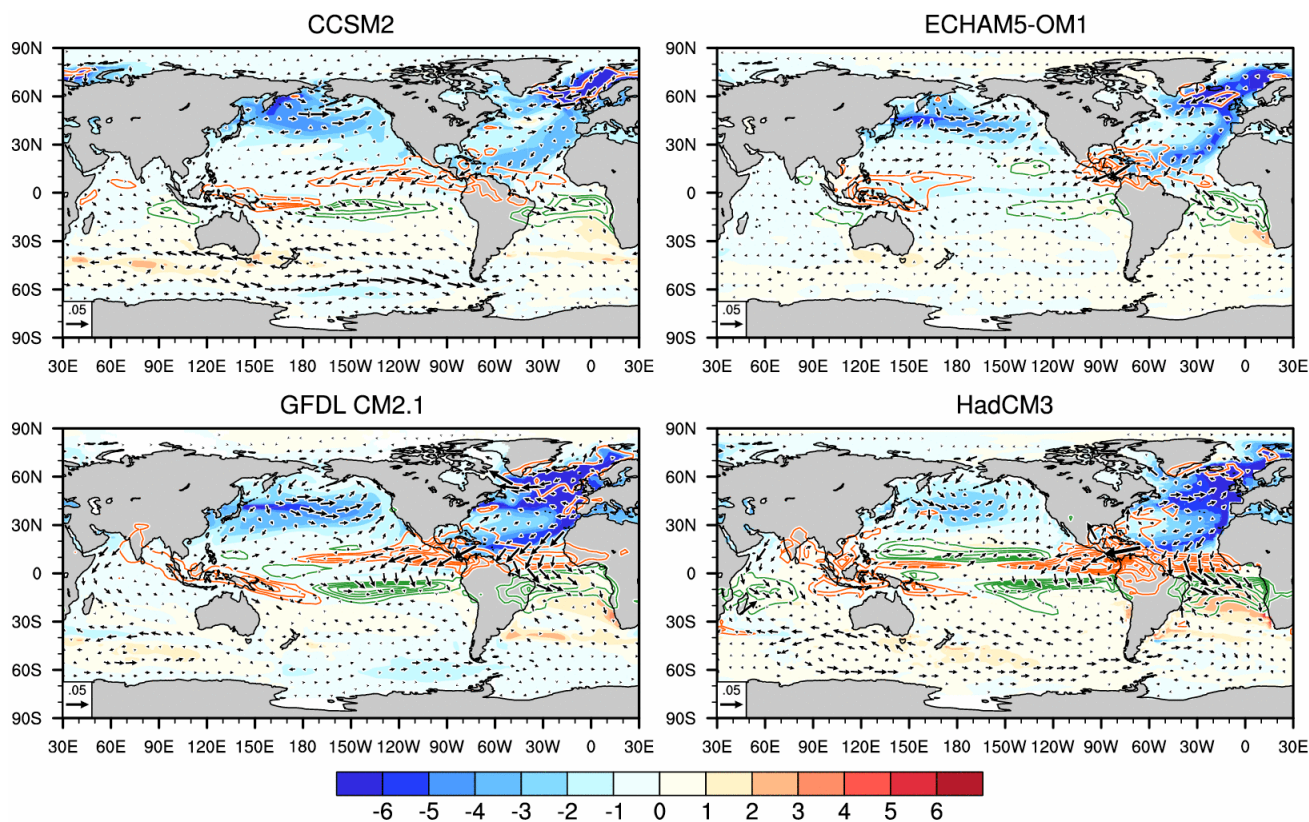


**Figure 1.** Ocean-atmosphere anomalies simulated by four different coupled GCMs in the 1-Sv water-hosing experiment. SST (shading; °C), surface wind stress (vectors;  $\text{N m}^{-2}$ ), and precipitation (green contours  $> 1 \text{ mm day}^{-1}$  and orange contours  $< -1 \text{ mm day}^{-1}$  at intervals of  $1 \text{ mm day}^{-1}$ ) anomalies are averaged over the last 30 years of the 100-year hosing period.

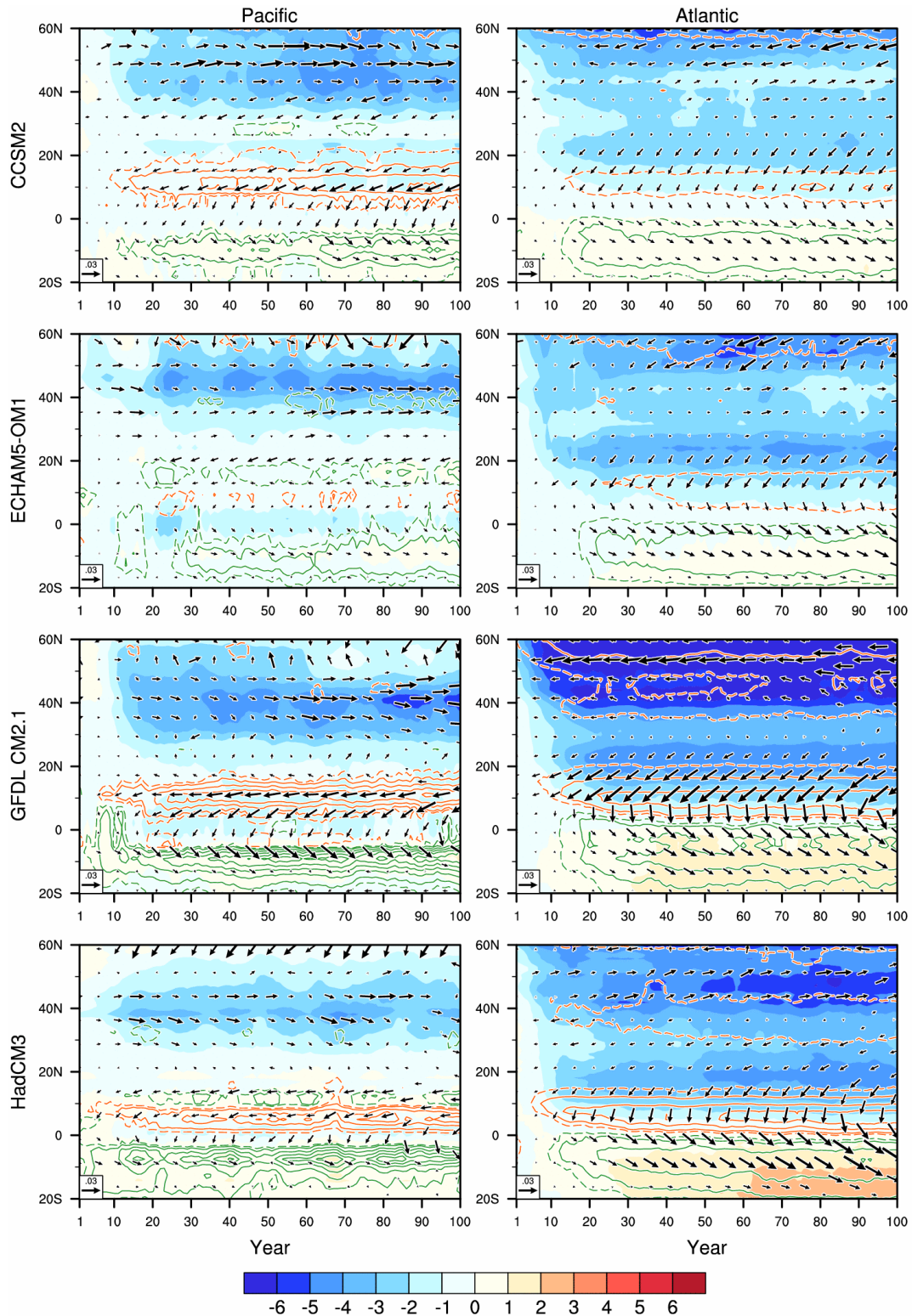


**Figure 2.** Time evolution of ocean-atmosphere anomalies simulated by four different coupled GCMs in the 1 Sv water-hosing experiment. SST (shading; °C), surface wind stress (vectors;  $\text{N m}^{-2}$ ), and precipitation (green contours  $> 1 \text{ mm day}^{-1}$  and orange contours  $< -1 \text{ mm day}^{-1}$  at intervals of  $1 \text{ mm day}^{-1}$ ; minor contours at  $+0.5/-0.5 \text{ mm day}^{-1}$  in dashed green/orange lines) anomalies are zonally averaged in (left) the Pacific ( $160^\circ\text{E}-150^\circ\text{W}$ ,  $>25^\circ\text{N}$ ;  $150^\circ\text{W}-100^\circ\text{W}$ ,  $<25^\circ\text{N}$ ) and (right) the Atlantic ( $60^\circ\text{W}-10^\circ\text{E}$ ) and smoothed with a 7-year running mean filter.

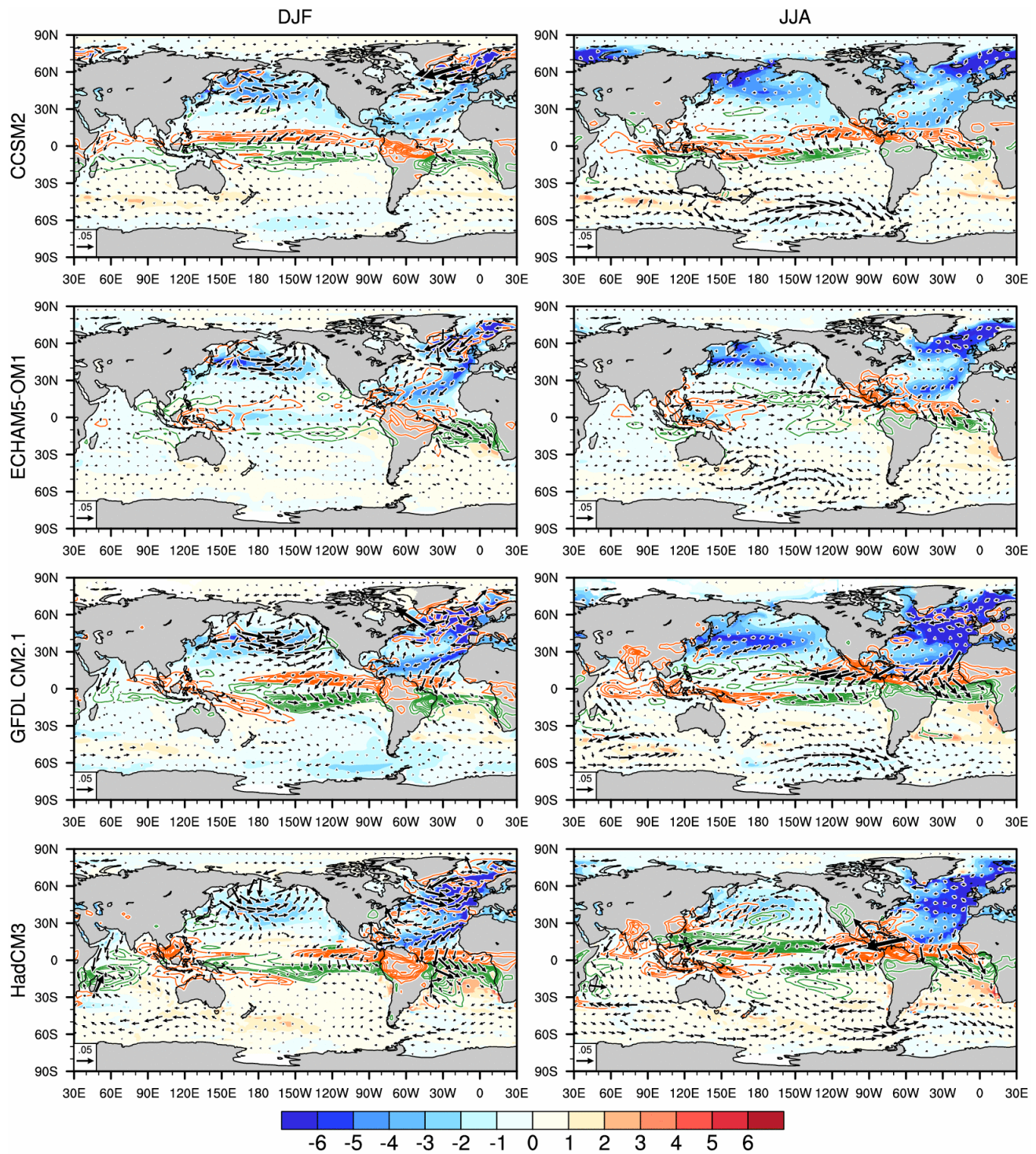


**Figure 3.** Same as in Fig. 1 but averaged in (left) December-February and (right) June-August.

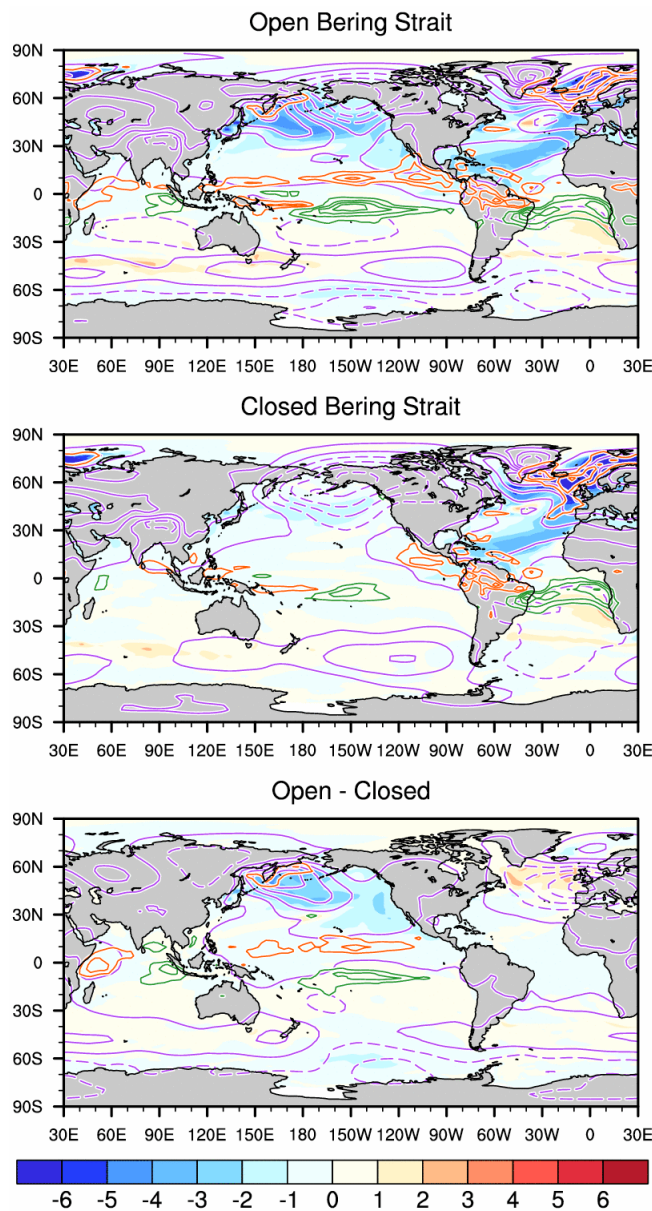


**Figure 4.** Ocean-atmosphere anomalies simulated by CCSM2 in (top) the open and (middle) closed Bering Strait 1-Sv water-hosing experiments and (bottom) their differences. SST (shading; °C), sea-level pressure (purple contours at intervals of 1 hPa; negative contours dashed), and precipitation (green contours  $> 1 \text{ mm day}^{-1}$  and orange contours  $< -1 \text{ mm day}^{-1}$  at intervals of  $1 \text{ mm day}^{-1}$ ) anomalies are averaged in October-March over the last 30 years of 100-year hosing period.

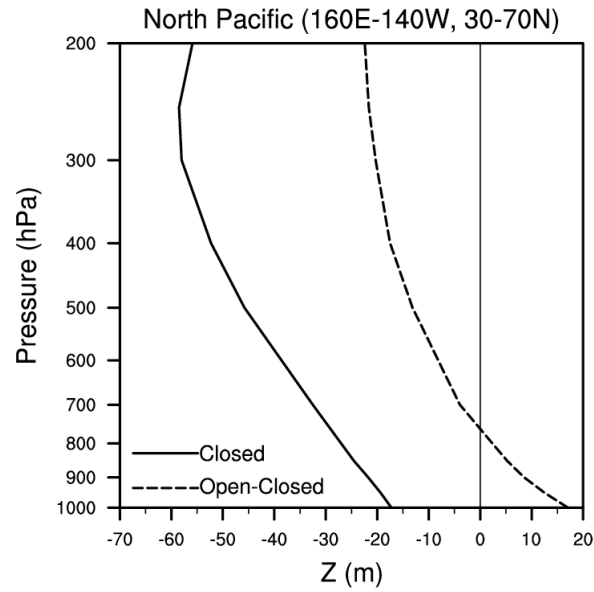


**Figure 5.** Vertical profiles of October-March geopotential height anomalies (m) over the Aleutian Low region (160°E-140°W, 30°-70°N) simulated by CCSM2 in the closed Bering Strait 1-Sv water-hosing experiment (solid) and the difference between the open and closed Bering Strait experiments (dashed).

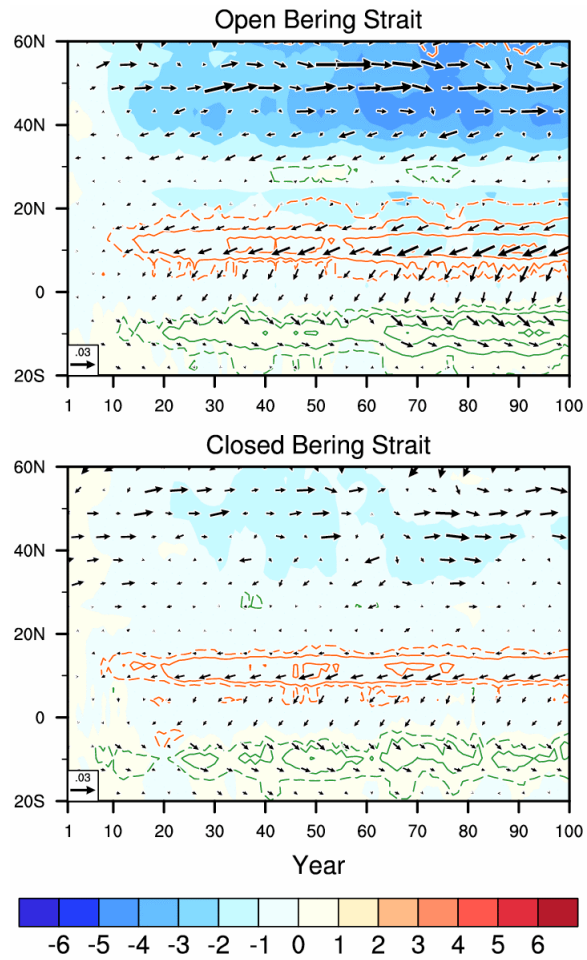


**Figure 6.** Same as in left panels of Fig. 2 but for anomalies simulated by CCSM2 in (top) the open and (bottom) closed Bering Strait 1-Sv water-hosing experiment. The top panel is repeated from Fig. 2.

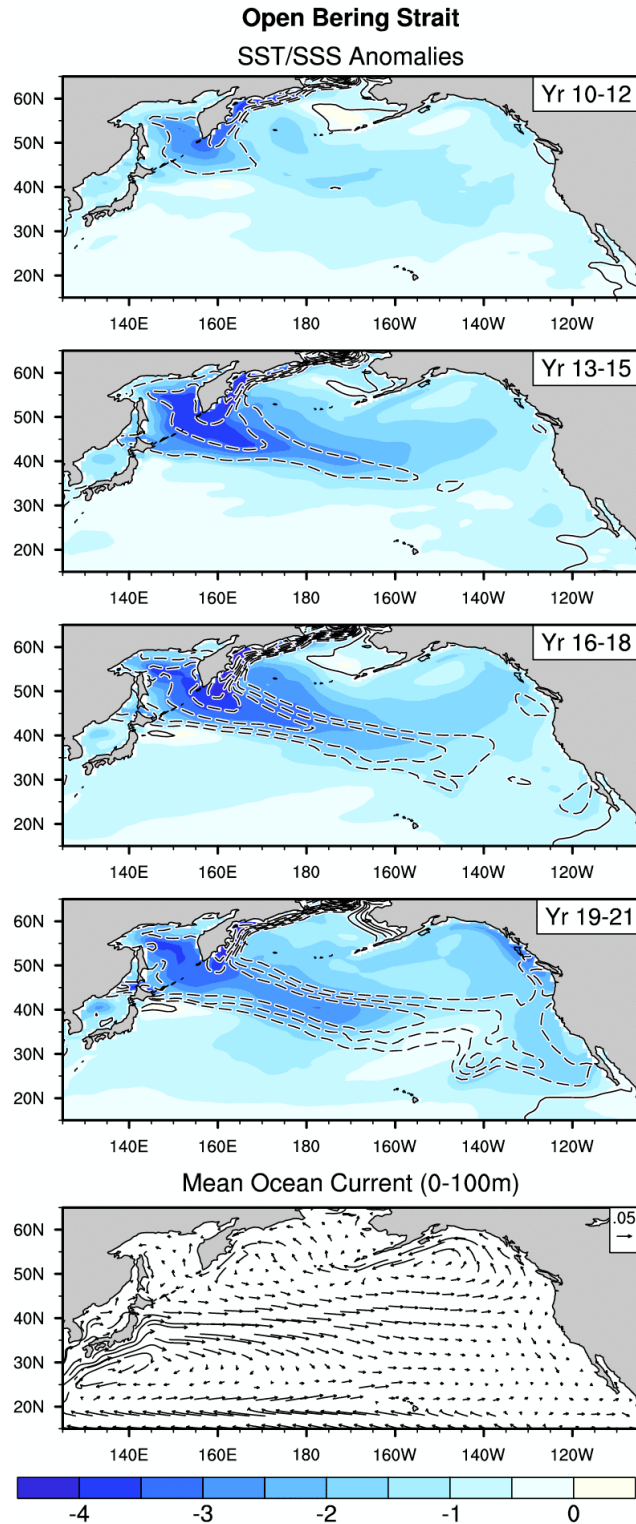


**Figure 7.** (top four) Time evolution of SST (shading; °C) and sea surface salinity (contours at intervals of 0.5 psu; negative contours dashed and zero contours omitted) anomalies simulated by CCSM2 in the open Bering Strait 1-Sv water-hosing experiment. Three-year average maps are shown from year 10-12 through year 19-21. (bottom) Mean ocean current ( $\text{m s}^{-1}$ ) in the control simulation of open Bering Strait experiment, averaged from the surface to 100 m depth over 200 years.

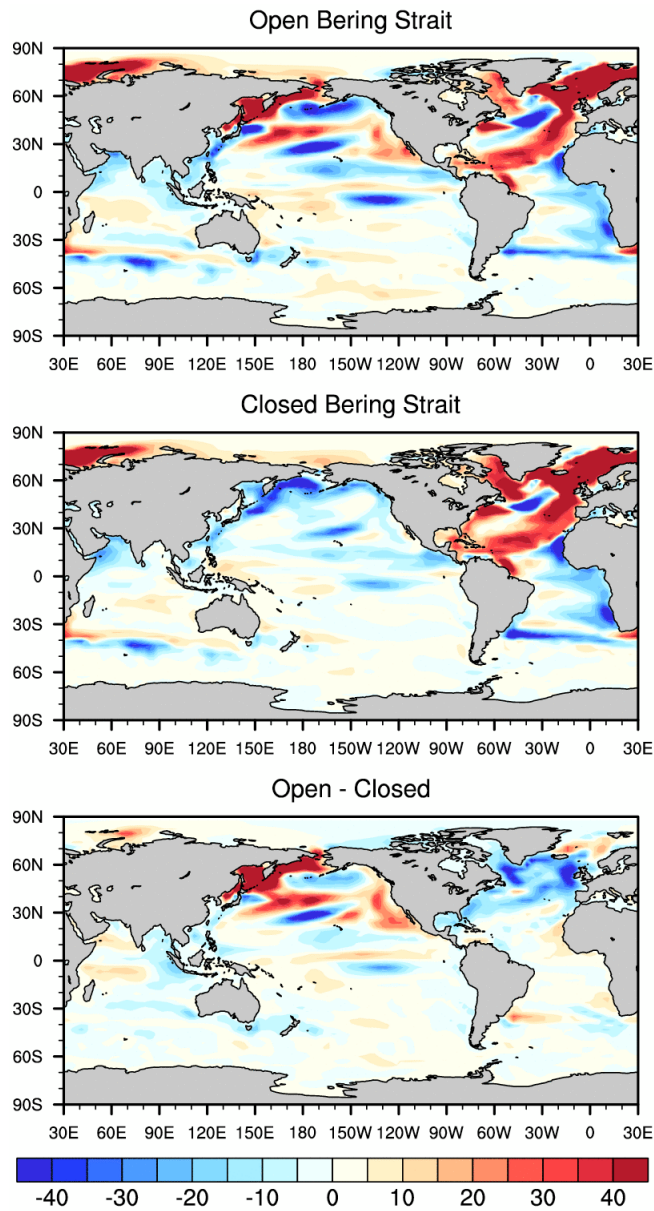


**Figure 8.** Same as in Fig. 4 but for the sum of latent and sensible heat flux anomalies ( $\text{W m}^{-2}$ ; downward positive).

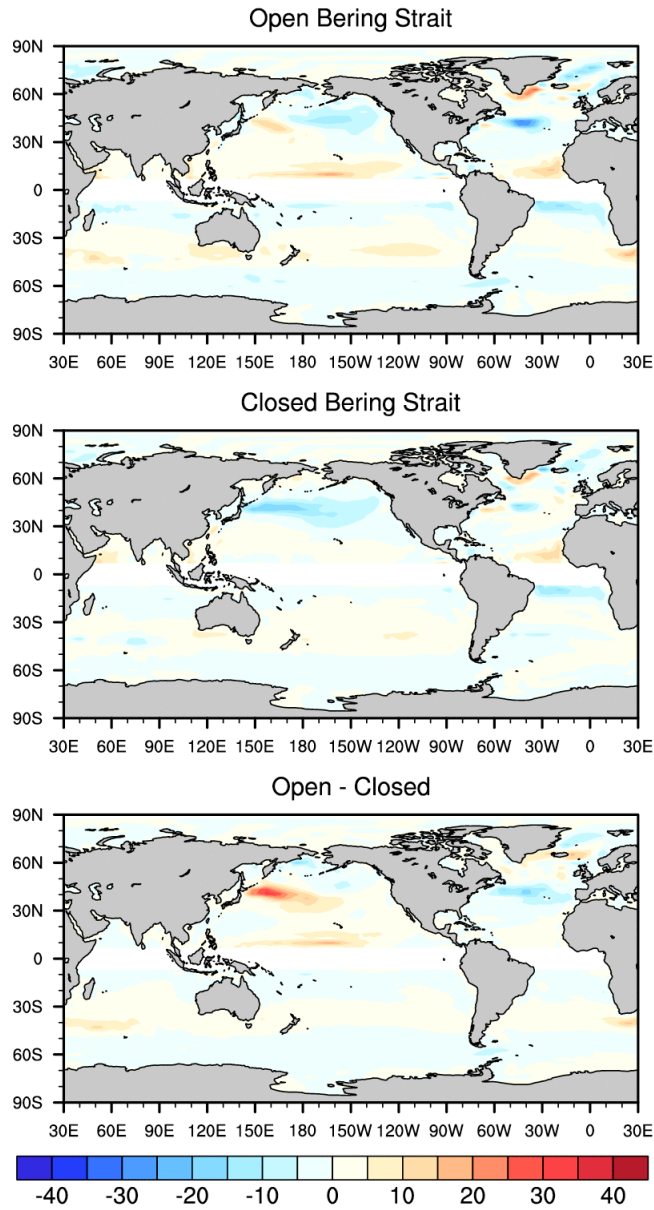


**Figure 9.** Same as in Fig. 4 but for the Ekman ocean heat transport anomalies ( $\text{W m}^{-2}$ ).

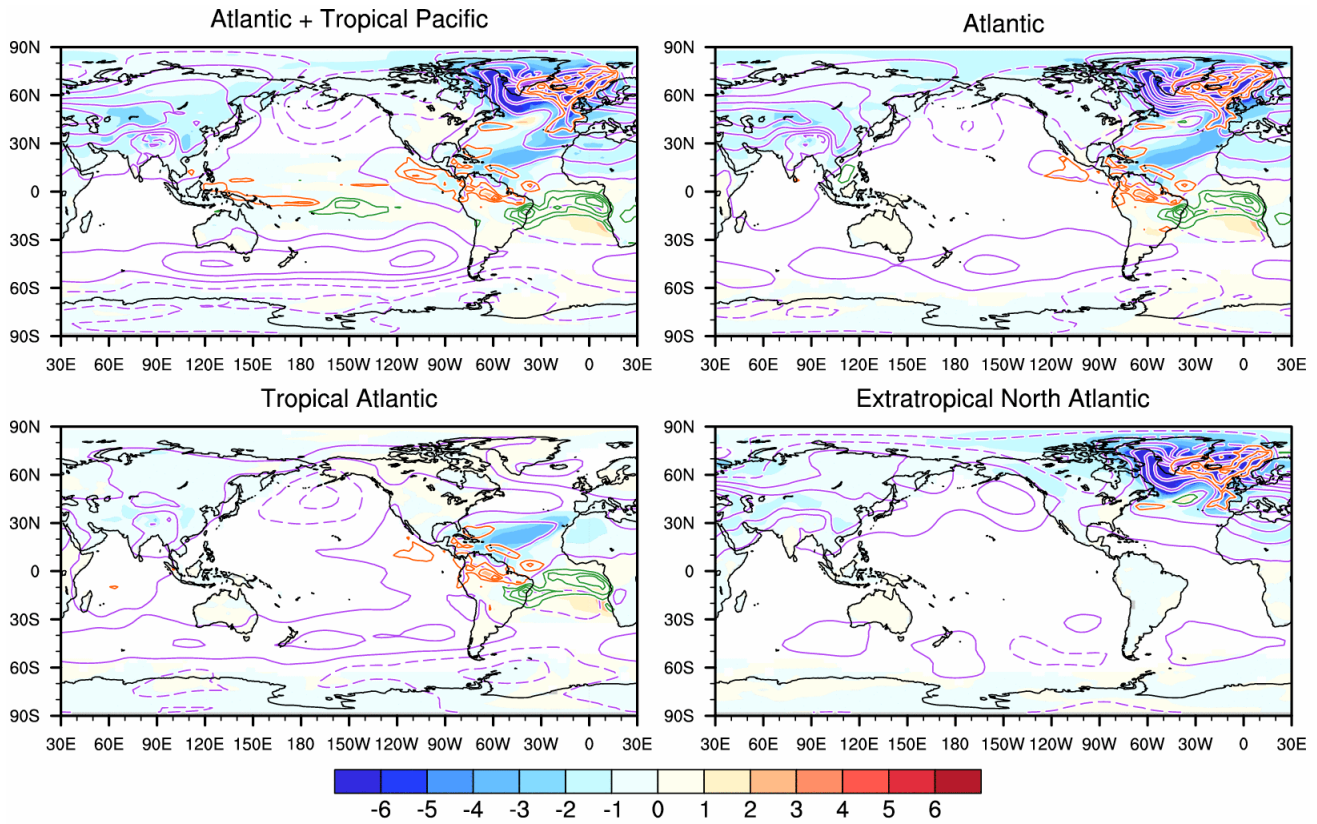


**Figure 10.** Atmospheric anomalies simulated by CAM2 forced with SST and sea ice anomalies from the CCSM2 closed Bering Strait experiment. SST and sea ice anomalies are prescribed over (top left) the Atlantic (25°S-75°N) and tropical Pacific (15°S-15°N), (top right) Atlantic (25°S-75°N), (bottom left) tropical Atlantic (25°S-30°N), and (bottom right) extratropical North Atlantic (40°-75°N). Surface temperature (shading; °C), sea-level pressure (purple contours at intervals of 1 hPa; negative contours dashed), and precipitation (green contours > 1 mm day<sup>-1</sup> and orange contours < -1 mm day<sup>-1</sup> at intervals of 1 mm day<sup>-1</sup>) anomalies are averaged over October-March.

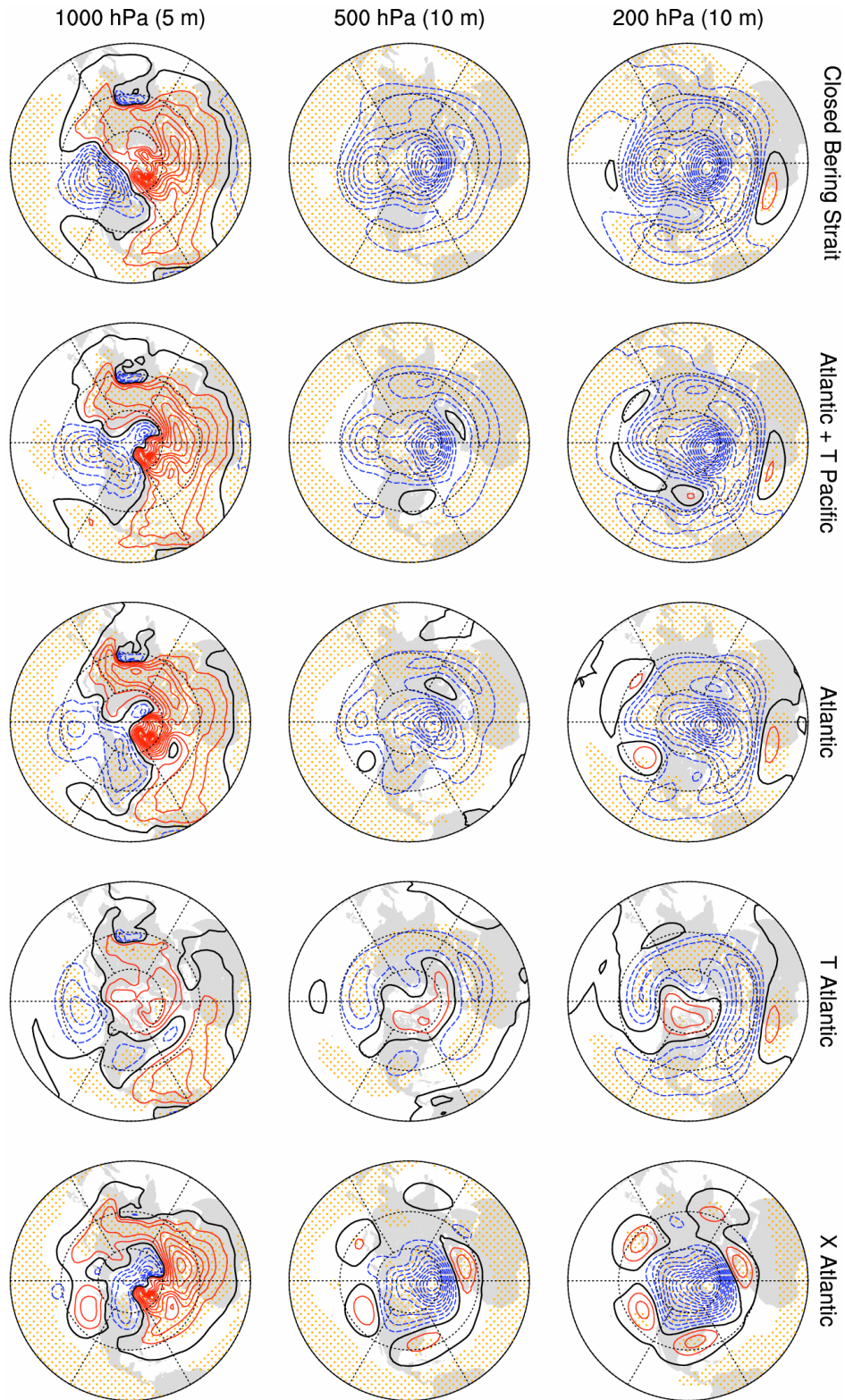


**Figure 11.** October-March geopotential height anomalies at 1000, 500, and 200 hPa (contours at intervals of 5, 10, and 10 m, respectively) simulated in (from left to right columns) the CCSM2 closed Bering Strait experiment and the CAM2 experiments forced with CCSM2's SST/sea ice anomalies over the Atlantic and tropical Pacific, Atlantic, tropical Atlantic, and extratropical North Atlantic. Orange stipples indicate the region of significant anomalies at the 98% level.

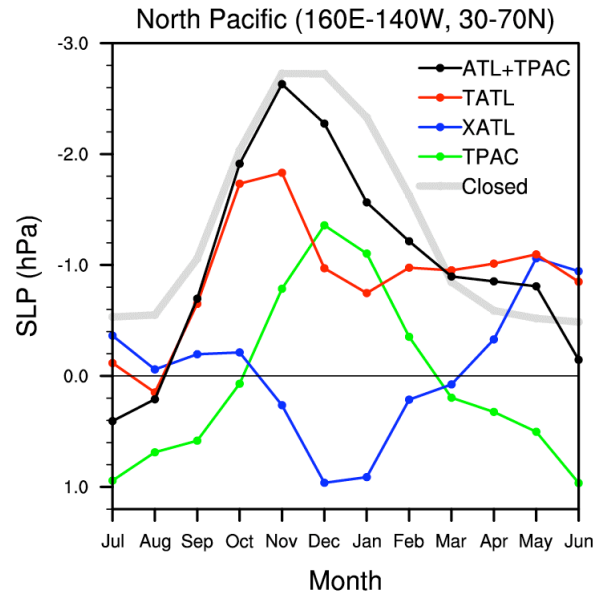


**Figure 12.** Sea-level pressure anomalies (hPa) averaged over the Aleutian Low region (160°E-140°W, 30°-70°N) as a function of calendar month. CCSM2 closed Bering Strait experiment (thick gray) and CAM2 experiments forced with CCSM2's SST/sea ice anomalies over the Atlantic and tropical Pacific (black), tropical Atlantic (red), extratropical North Atlantic (blue), and tropical Pacific (green; estimated by taking the difference between the Atlantic + tropical Pacific and Atlantic runs).

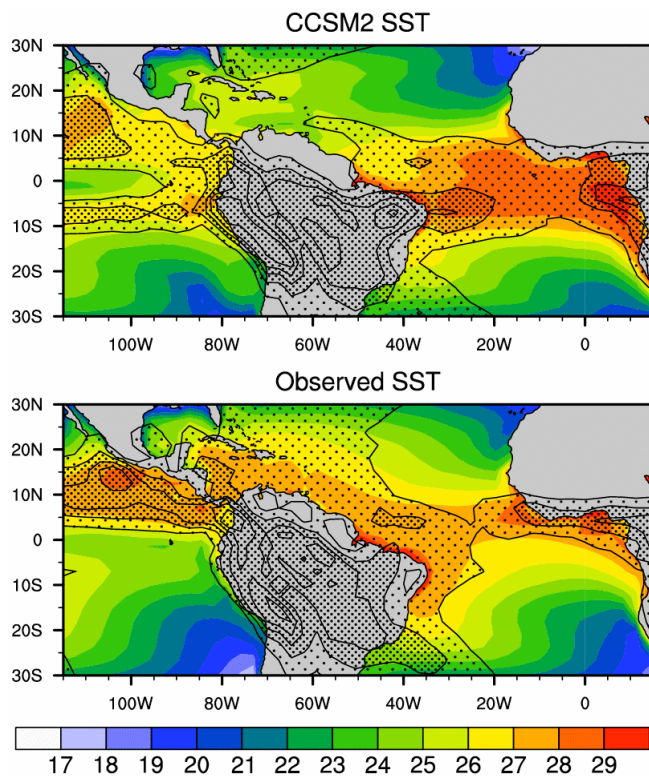


**Figure 13.** (top) SST climatology simulated in the control run of CCSM2 closed Bering Strait experiment (shading; °C) and mean precipitation simulated in CAM2 forced with this SST climatology (contours at intervals of 2 mm day<sup>-1</sup>; stippled > 2 mm day<sup>-1</sup>). (bottom) Same as in the top panel but for observed SST climatology (HadISST, 1942-2001) and mean precipitation simulated in CAM2 forced with this SST. All fields are shown for October-March.

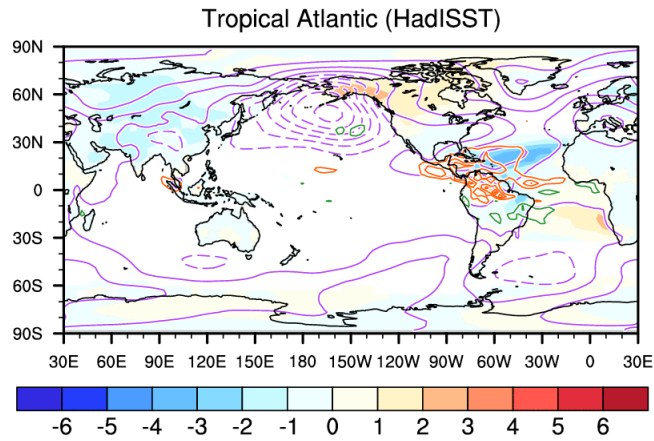


**Figure 14.** Same as in the bottom left panel of Fig. 10 but the climatological SST field has been replaced with observational data (HadISST).